

COPY RESOLUTION TEST CHART

DTIC FILE COPY

14

**RADC-TR-86-151
In-House Report
October 1986**



AD-A179 170

RECTANGULAR MICROSTRIP PATCH ANTENNA ARRAYS

Daniel A. Mullinix, 2Lt, USAF and Daniel T. McGrath, Capt, USAF

APPROVED FOR PUBLIC RELEASE; DISTRIBUTION UNLIMITED

DTIC
S E D
APR 20 1987
E

**ROME AIR DEVELOPMENT CENTER
Air Force Systems Command
Griffiss Air Force Base, NY 13441-5700**

87 4 17 083

This report has been reviewed by the RADC Public Affairs Office (PA) and is releasable to the National Technical Information Service (NTIS). At NTIS it will be releasable to the general public, including foreign nations.

RADC-TR-86-151 has been reviewed and is approved for publication.

APPROVED:



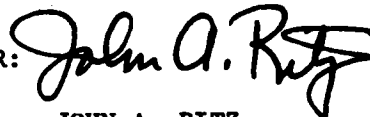
JOHN K. SCHINDLER
Chief, Antennas & RF Components Branch
Electromagnetic Sciences Division

APPROVED:



PAUL J. FAIRBANKS, Lt Colonel, USAF
Deputy Chief, Electromagnetic Sciences Division

FOR THE COMMANDER:



JOHN A. RITZ
Plans and Programs Division

If your address has changed or if you wish to be removed from the RADC mailing list, or if the addressee is no longer employed by your organization, please notify RADC (EEAA) Griffiss AFB NY 13441-5700. This will assist us in maintaining a current mailing list.

Do not return copies of this report unless contractual obligations or notices on a specific document requires that it be returned.

UNCLASSIFIED

SECURITY CLASSIFICATION OF THIS PAGE

REPORT DOCUMENTATION PAGE				
1a. REPORT SECURITY CLASSIFICATION UNCLASSIFIED		1b. RESTRICTIVE MARKINGS AD-A179170		
2a. SECURITY CLASSIFICATION AUTHORITY		3. DISTRIBUTION / AVAILABILITY OF REPORT		
2b. DECLASSIFICATION / DOWNGRADING SCHEDULE		Approved for Public Release; Distribution Unlimited.		
4. PERFORMING ORGANIZATION REPORT NUMBER(S) RADC-TR-86-151		5. MONITORING ORGANIZATION REPORT NUMBER(S)		
6a. NAME OF PERFORMING ORGANIZATION Rome Air Development Center		6b. OFFICE SYMBOL (if applicable) RADC/EEAA	7a. NAME OF MONITORING ORGANIZATION Rome Air Development Center	
6c. ADDRESS (City, State, and ZIP Code) Hanscom AFB Massachusetts, 01731		7b. ADDRESS (City, State, and ZIP Code) Hanscom AFB Massachusetts, 01731		
8a. NAME OF FUNDING / SPONSORING ORGANIZATION Rome Air Development Center		8b. OFFICE SYMBOL (if applicable) RADC/EEAA	9. PROCUREMENT INSTRUMENT IDENTIFICATION NUMBER	
8c. ADDRESS (City, State, and ZIP Code) Hanscom AFB Massachusetts, 01731		10. SOURCE OF FUNDING NUMBERS		
		PROGRAM ELEMENT NO. 62702F	PROJECT NO. 4600	TASK NO. 14
				WORK UNIT ACCESSION NO. 02
11. TITLE (Include Security Classification) (U) Rectangular Microstrip Patch Antenna Arrays				
12. PERSONAL AUTHOR(S) Daniel A. Mullinix, 2Lt, USAF; Daniel T. McGrath, Capt, USAF				
13a. TYPE OF REPORT In-house		13b. TIME COVERED FROM Oct 85 to May 86	14. DATE OF REPORT (Year, Month, Day) 1986 October	15. PAGE COUNT 54
16. SUPPLEMENTARY NOTATION				
17. COSATI CODES			18. SUBJECT TERMS (Continue on reverse if necessary and identify by block number)	
FIELD 09	GROUP 03	SUB-GROUP	Microstrip Antennas Microwave Components	
			Conformal Antennas Printed Circuit Antennas	
19. ABSTRACT (Continue on reverse if necessary and identify by block number) This report is oriented toward designing rectangular microstrip patch antenna arrays with corporate feed networks. It includes an explanation of the transmission line model for designing inset feed rectangular patch antennas and presents some very accurate results that were achieved in spite of the relative simplicity of the model. In addition, it presents a reactive power divider design that doesn't require much space, yet was near ideal in minimizing the input VSWR and providing equal phase and amplitude between the output ports. Finally, it presents a 4x4 array designed for 8 GHz which achieved near maximum gain with very little phase or amplitude error...				
20. DISTRIBUTION / AVAILABILITY OF ABSTRACT <input type="checkbox"/> UNCLASSIFIED/UNLIMITED <input checked="" type="checkbox"/> SAME AS RPT. <input type="checkbox"/> DTIC USERS			21. ABSTRACT SECURITY CLASSIFICATION Unclassified	
22a. NAME OF RESPONSIBLE INDIVIDUAL Daniel A. Mullinix 2Lt, USAF		22b. TELEPHONE (Include Area Code) (617) 377-4036	22c. OFFICE SYMBOL RADC/EEAA	

DD FORM 1473, 84 MAR

83 APR edition may be used until exhausted.
All other editions are obsolete.

SECURITY CLASSIFICATION OF THIS PAGE

UNCLASSIFIED

DISCLAIMER NOTICE

THIS DOCUMENT IS BEST QUALITY PRACTICABLE. THE COPY FURNISHED TO DTIC CONTAINED A SIGNIFICANT NUMBER OF PAGES WHICH DO NOT REPRODUCE LEGIBLY.

Contents

1. INTRODUCTION	1
2. RECTANGULAR MICROSTRIP PATCH ANTENNAS	2
2.1 The Transmission Line Model	2
2.2 Inset Feed Rectangular Patch	5
3. RECTANGULAR PATCH ANTENNA TEST RESULTS	8
3.1 Resonant Frequency	8
3.2 Return Loss	11
3.3 Radiation Patterns	12
3.4 Bandwidth	13
4. REACTIVE POWER DIVIDERS	13
5. PATCH ARRAY WITH INTEGRAL CORPORATE FEED	18
6. CONCLUSIONS AND RECOMMENDATIONS	23
REFERENCES	26
APPENDIX A: PATCH RADIATION PATTERNS	27

Accession For	
NTIS GRA&I	<input checked="" type="checkbox"/>
DTIC TAB	<input type="checkbox"/>
Unannounced	<input type="checkbox"/>
Justification	
By _____	
Distribution/	
Availability Codes	
Dist	Avail and/or Special
A-1	23 JK

iii



Illustrations

1. Edge Fed Rectangular Patch Antenna	3
2. Equivalent Circuit for Patch Input Admittance	4
3. Inset Feed Rectangular Patch Antenna	6
4. Equivalent Circuit for the Inset Feed Patch	7
5. Variation of Patch Input Admittance with Patch Length b/λ	8
6. Photograph of the 6 GHz Patch Mounted in the Test Fixture	9
7. Measured Resonant Frequency vs. Design Frequency	10
8. Resonant Frequency vs. Patch Length for Measured Data and Original and Modified Transmission Line Models	11
9. Typical Return Loss vs. Frequency (Measured)	12
10. Measured Attenuation (db/inch) of a Microstripline on Epoxy	13
11. Return Loss of the Experimental Patch Antennas	14
12. Typical Radiation Patterns (8 GHz Patch): (a) E Plane, (b) H Plane	15
13. Measured Bandwidth of the Experimental Patch Antennas	16
14. Power Divider Mounted in Test Fixture	17
15. Fringing Fields of Microstrip Transmission Line	18
16. Return Loss of the Experimental Power Dividers at Input Port and Output Ports	19
17. Amplitude Balance in the Experimental Power Dividers	20
18. Insertion Loss, Net Power Loss and Isolation in the Experimental Power Dividers	21
19. Microstrip Array Antenna with Integral Corporate Feed (8 GHz, $\epsilon_r=2.55$, $h=1/16"$)	22
20. Measured Return Loss of the Experimental 4x4 Array	23
21. Measured E Plane Pattern of the Experimental 4x4 Array	24
22. Stagger-Tuned Patch: (a) Geometry, (b) Model	25
23. Arbitrary Patch Geometry	25

Rectangular Microstrip Patch Antenna Arrays

1. INTRODUCTION

Microstrip (printed circuit) antennas are low in cost, relatively easy to construct and are very lightweight. Those properties make them ideal for aircraft and satellite antennas, and as experimental hardware for testing new antenna concepts. Rome Air Development Center (RADC) has become involved in this technology area for two major reasons: (1) to verify and augment existing design models that will be used in developing millimeter wave antennas for airborne and satellite communications terminals; and (2) to build an in-house capability to rapidly provide antennas to support other RADC experiments.

Previous phases of this program have focused on verifying printed circuit transmission line designs and transitions from those lines to coaxial cable¹, and on printed circuit power dividers for amplitude tapering of array antennas². The present effort is oriented toward designing rectangular patch arrays with integral corporate feed networks.

(Received for Publication 7 Oct 1986)

1. Kozak, F.E. and McGrath, D.T. (1985) Printed Circuit Transmission Line Transitions, RADC-TR-85-241, AD A169291.
2. Huck, K.D. (1986) Microstrip Amplitude-Weighted Wilkinson Power Dividers, RADC-TR-85-275, AD A169450.

This report will present experimental measurements of inset-fed rectangular patch antennas, microstrip power dividers, and the combination of those into planar microstrip arrays. The most significant results of this work are: (1) the transmission line model accurately predicts the patch resonant frequency for given dimensions for patches with coplanar feed lines, in spite of its relative simplicity compared to other models; (2) a simple form of reactive power divider is adequate for array antennas; and (3) a 4x4 array designed for 8.0 GHz achieved very near the maximum possible gain and had very little phase or amplitude error in the feed lines, power dividers or array elements.

2. RECTANGULAR MICROSTRIP PATCH ANTENNA

2.1 The Transmission Line Model

A rectangular patch antenna with a coplanar feed line is shown in Figure 1. It has width and length of a and b , respectively, and thickness t . It is on the top of a dielectric sheet whose thickness is h . In the transmission line model, this antenna is modeled as two slots centered on the two edges of the patch perpendicular to the feed line. The slots are assumed to have width h and lengths a and $(a-w)$. Harrington gives the admittance of a narrow h -plane slot as³:

$$Y = \frac{\pi a}{\lambda \eta_0} \left(1 - \frac{k^2 h^2}{24}\right) + j \frac{a}{\lambda \eta_0} [3.135 - 2 \ln(kh)] \quad (1)$$

$$= G_s + jB_s$$

Since the slot on the feed side of the patch is partially blocked by the feed line, its admittance is found simply by replacing a with $(a-w)$ in (1). The above formula is only strictly valid for substrate thicknesses $h < .1\lambda$. For thicker substrates, the admittance may be found using the following elliptic integrals³:

$$\lambda \eta_0 G_s = 2 \int_0^{kh/2} \frac{\sin^2 \omega \, d\omega}{\omega^2 \sqrt{(kh/2)^2 - \omega^2}} \quad (2a)$$

3. Harrington, R.F. (1961) Time-Harmonic Electromagnetic Fields, McGraw-Hill.

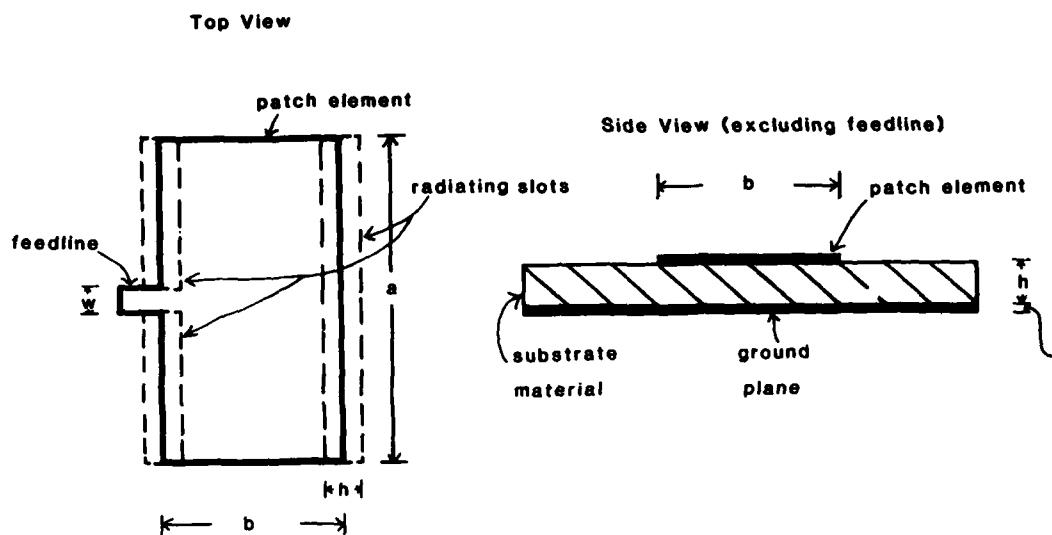


Figure 1. Edge Fed Rectangular Patch Antenna

$$\lambda \eta_0 B_s = 2 \int_0^{\infty} \frac{\sin^2 \omega d \omega}{\omega^2 \sqrt{\omega^2 - (kh/2)^2}} \quad (2b)$$

The patch itself is modeled as a section of microstrip transmission line of width a . Its admittance can be approximated (for $a \gg h$) by the formula

$$Y_p \approx \frac{a \sqrt{\epsilon_r}}{h \eta_0} \quad (3)$$

where η_0 is 376.7Ω , the impedance of free space. Since the substrate is usually thin, relative to the wavelength, (3) is almost always valid. However, for cases of electrically thick substrates, the following formula given by Schaubert et. al. is more accurate, since it accounts for the fringing fields along the edge of the patch parallel to the feed line⁴:

$$Y_p = \frac{\sqrt{\epsilon_r} e}{\eta_0} \left[\frac{a}{h} + 1.393 + .667 \ln \left(\frac{a}{h} + 1.444 \right) \right]^{-1} \quad (4a)$$

4. Schaubert, D.H., Farrar, F.G., Sindoris, A. and Hayes, S.T. (1981) "Microstrip Antennas with Frequency Agility and Polarization Diversity," IEEE Transactions on Antennas and Propagation, AP-29, pp. 118-123.

$$\text{where } \epsilon_e = \frac{\epsilon_r + 1}{2} + \frac{\epsilon_r - 1}{2\sqrt{1 + 10t/h}} \quad (4b)$$

Regardless of which formula is used for Y_p , the input admittance, Y_{in} , is the admittance of the first slot in parallel with the admittance of the second slot transformed back to the feed point. Figure 2 is an equivalent circuit. The input admittance is expressed as:

$$Y_{in} = Y_{s1} + \hat{Y}_{s2} \quad (5)$$

where \hat{Y}_{s2} is the series admittance of the patch and the second slot looking into the feed point, or the admittance of the second slot transformed back to the feed point. On the open circuit side of the patch (the side opposite the feed), the reflection coefficient ρ_2 is

$$\rho_2 = (Y_{s2} - Y_p) / (Y_{s2} + Y_p) \quad (6)$$

and therefore \hat{Y}_{s2} can be written as:

$$\hat{Y}_{s2} = Y_p \frac{e^{jk\ell} + \rho_2 e^{-jk\ell}}{e^{jk\ell} - \rho_2 e^{-jk\ell}} \quad (7)$$

where ℓ is the electrical length of the patch, $\ell = b\sqrt{\epsilon_r}$. If we express Y_{s1} and Y_{s2} as, respectively, $G_1 + jB_1$ and $G_2 + jB_2$ and also use Euler's relations, we can combine (5) and (7) into a final expression for the input admittance:

$$Y_{in} = G_1 + jB_1 + \left\{ \frac{Y_p G_2 \cos(k\ell) + j[B_2 \cos(k\ell) + Y_p \sin(k\ell)]}{[Y_p \cos(k\ell) - B_1 \sin(k\ell)] + jG_1 \sin(k\ell)} \right\} \quad (8)$$

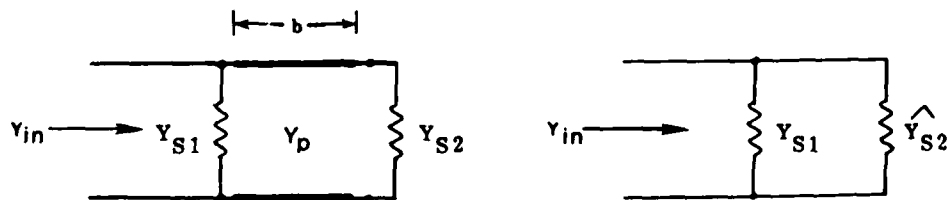


Figure 2. Equivalent Circuit for Patch Input Admittance

The resonant frequency corresponds to that value of $k=2\pi/\lambda$ that makes the imaginary part of (8) equal zero, or the part in braces equal to $-jB_1$. For substrates that are very thin relative to a wavelength, the patch length is typically around $.49\lambda_0/\sqrt{\epsilon_r}$.

After determining the correct patch length for a chosen frequency, we must then match the feed line's characteristic impedance to the real part of (8). Unfortunately, the resistance at the edge of a typical patch varies from about 250Ω for a square patch, to about 150Ω for a patch with an aspect ratio of $1.3=a/b$ ⁵. It is not always convenient to use feed lines with such high characteristic impedances. The most practical way to reduce that input resistance at resonance is to inset the feed line into the patch, as discussed in the next section.

2.2 Inset Feed Rectangular Patch

To use a feed line with a lower characteristic impedance, Z_0 , we move the feed point inward from the patch edge by cutting two short slots parallel to the feed line, as shown in Figure 3, thus forming an inset feed. The patch input impedance varies from zero at the center to a high value at the edge. Carver and Mink⁵ give an approximate expression for the input resistance as a function of the feed point and edge resistance, from which we have derived the following expression for the length, d , of the inset:

$$d = (b/\pi) \cos^{-1} [R_0/\sqrt{R_e}] \quad (9)$$

where R_0 equals Z_0 , the characteristic impedance of the feed line, and R_e is the edge input resistance of the patch without an inset feed. To obtain more accurate results, we have modified our transmission line model as described below.

For an inset feed patch, the input admittance is evaluated by transforming both slot admittances to the location of the feed point, as shown in the equivalent circuit of Figure 4. On the open circuit side of the patch, the reflection coefficient is still as given in (6), and that of the feed side will be similar. The transformed admittances are then:

$$\hat{Y}_{s1} = Y_p \frac{\exp(jk\ell_1) + \rho_1 \exp(-jk\ell_1)}{\exp(jk\ell_1) - \rho_1 \exp(-jk\ell_1)} ; \quad \rho_1 = (Y_{s1} - Y_p) / (Y_{s1} + Y_p) \quad (10a)$$

5. Carver, K.R. and Mink, J.W. (1981) "Microstrip Antenna Technology," IEEE Transactions on Antennas and Propagation, AP-29, pp. 1-24.

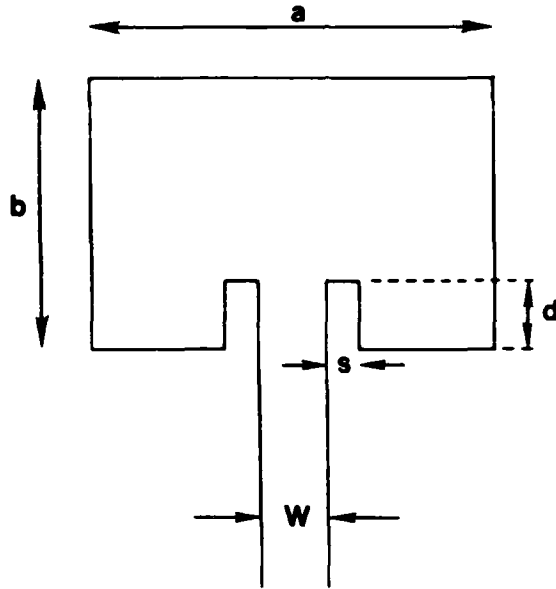


Figure 3. Inset Feed Rectangular Patch Antenna

$$\hat{Y}_{s2} = Y_p \frac{\exp(jk\ell_2) + \rho_2 \exp(-jk\ell_2)}{\exp(jk\ell_2) - \rho_2 \exp(-jk\ell_2)} ; \quad \rho_2 = (Y_{s2} - Y_p) / (Y_{s2} + Y_p) \quad (10b)$$

Adding the two admittances in parallel, and using Euler's relations, we obtain the following expression for the input admittance:

$$\frac{Y_{in}}{Y_p} = \frac{G_1 \cos(k\ell_1) + j[B_1 \cos(k\ell_1) + Y_p \sin(k\ell_1)]}{[Y_p \cos(k\ell_1) - B_1 \sin(k\ell_1)] + jG_1 \sin(k\ell_1)} + \frac{G_2 \cos(k\ell_2) + j[B_2 \cos(k\ell_2) + Y_p \sin(k\ell_2)]}{[Y_p \cos(k\ell_2) - B_2 \sin(k\ell_2)] + jG_2 \sin(k\ell_2)} \quad (11)$$

where $\ell_1 = d\sqrt{\epsilon_r}$, $\ell_2 = (b-d)\sqrt{\epsilon_r}$, $k = 2\pi/\lambda_0$, and G_1 , B_1 , G_2 and B_2 are given by (1). Figure 5 shows the variation of the real and imaginary parts of the input impedance with patch length for a given frequency.

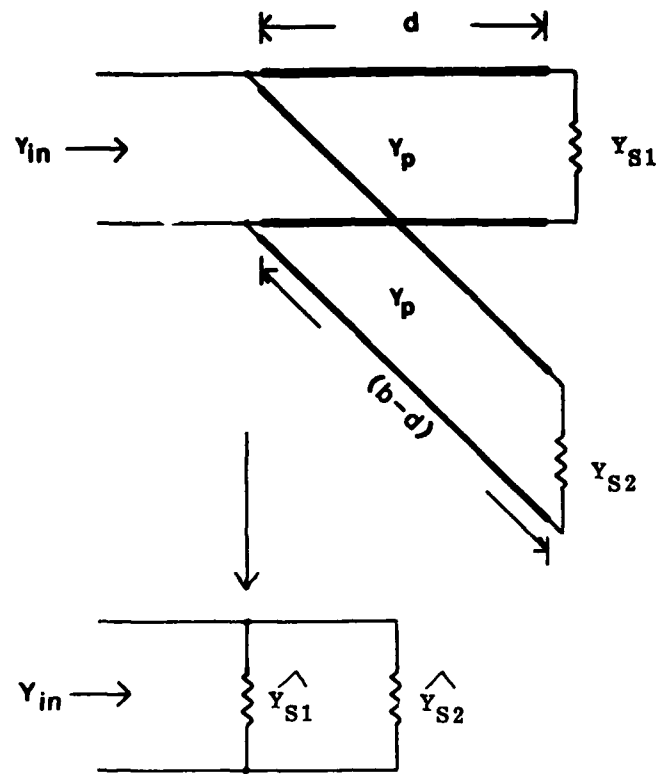


Figure 4. Equivalent Circuit for the Inset Feed Patch

To determine the correct patch dimensions for a given resonant frequency and input impedance, we set $d=0$ in (11) and make successive guesses at b until the imaginary part equals zero. A good initial guess is $b = .49\lambda_0 / \sqrt{\epsilon_r}$. Next, we adjust d until the real part equals the feed line's characteristic impedance, using (9) as an initial guess. Note that the admittance of the first slot depends on the width, w , of the feed line. Gupta et. al.⁶ give formulas for calculating the microstrip line width for a given characteristic impedance.

The design equations for inset feed rectangular patches and microstrip transmission lines have been incorporated into a computer subroutine library⁷. Also included in that library are routines that use the Calcomp® plotter to produce accurate, high-quality mask artwork. The drawings are usually made at 2x scale, then photographically reduced to produce the negative that is used in photoetching the printed circuit.

6. Gupta, K.C., Garg, R. and Chadha, R. (1980) Computer Aided Design of Microwave Circuits, Artech House.
7. McGrath, D.T., Mullinix, D.A. and Huck, K.D. (1986) Fortran Subroutines for Design of Printed Circuit Antennas, RAD-86-08.

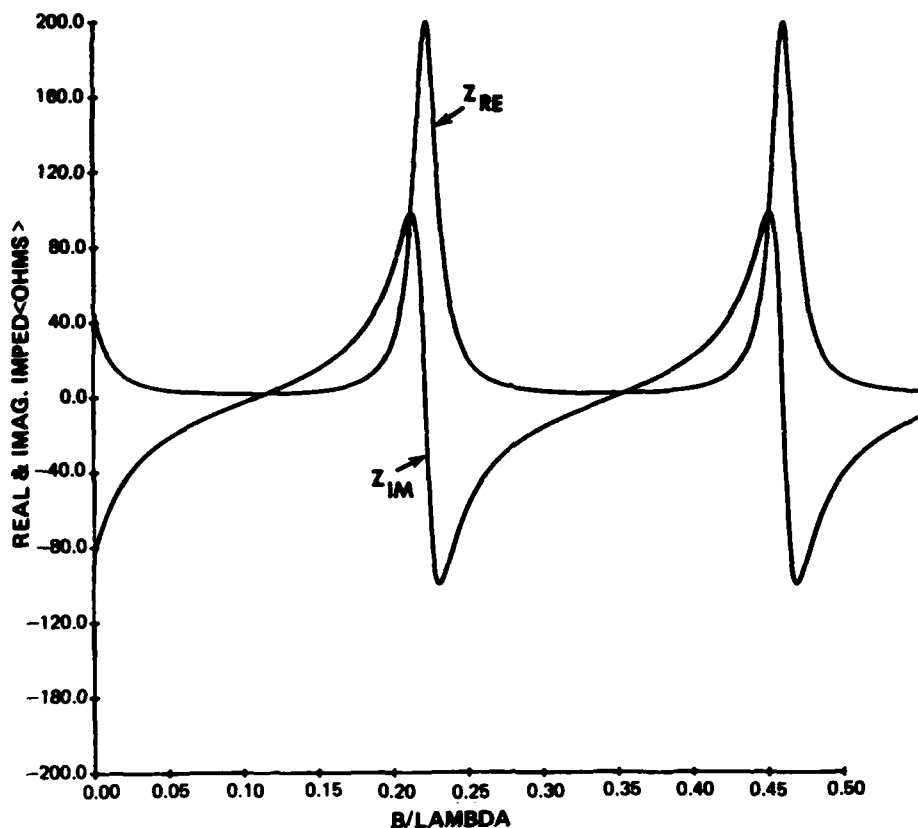


Figure 5. Variation of Patch Input Admittance with Patch Length b/λ .

3. RECTANGULAR PATCH ANTENNA TEST RESULTS

3.1 Resonant Frequency

Seventeen individual patch antennas with resonant frequencies between 2 and 18 GHz were constructed and tested. Figure 6 is a photograph of one of the antennas in its test fixture. The substrate material was 1/16" thick epoxy-fiberglass with a dielectric constant of 4.4 and 1-oz. Copper cladding ($t=.0014$ "). Figure 7 shows the design frequency versus the measured resonant frequency. It is apparent from that graph that the original model is accurate up to 13 GHz, which corresponds to $b/h=3.0$. With increasing frequency above 13 GHz, the measured resonant frequencies were progressively farther below the design frequencies. A combination of two errors in the original model caused this discrepancy: first, the electrical distance between the patch edges depends on the effective dielectric constant; and second, fringing at the radiating edges of the patch causes it to appear electrically longer than b .

Section 4 of this report discusses the effective dielectric constant in detail as it pertains to power divider design. Its importance to the patch model is that the electrical distance between the radiating edges depends on the propagation velocity within the patch section, and that is not simply a function of the relative permittivity, but varies with the patch width and the operating frequency. For very wide transmission lines ϵ_{eff} is very nearly the same as ϵ_r , which explains why our model is more accurate at low frequencies - those patches are very wide. But at high frequencies the patch is narrow enough for the difference between ϵ_r and ϵ_{eff} to be appreciable.

In addition, we had earlier assumed the radiating "slots" to be centered at the edge of the patch. However, fringing at the radiating edges will cause those to appear electrically some small distance beyond the edge. Hammerstad gives a very good approximation for apparent length extension of an open-circuited microstrip transmission line as ⁶:

$$\Delta l = .412h \frac{(\epsilon_{\text{eff}} + .3) (W/h + .264)}{(\epsilon_{\text{eff}} - .258) (W/h + .8)}$$

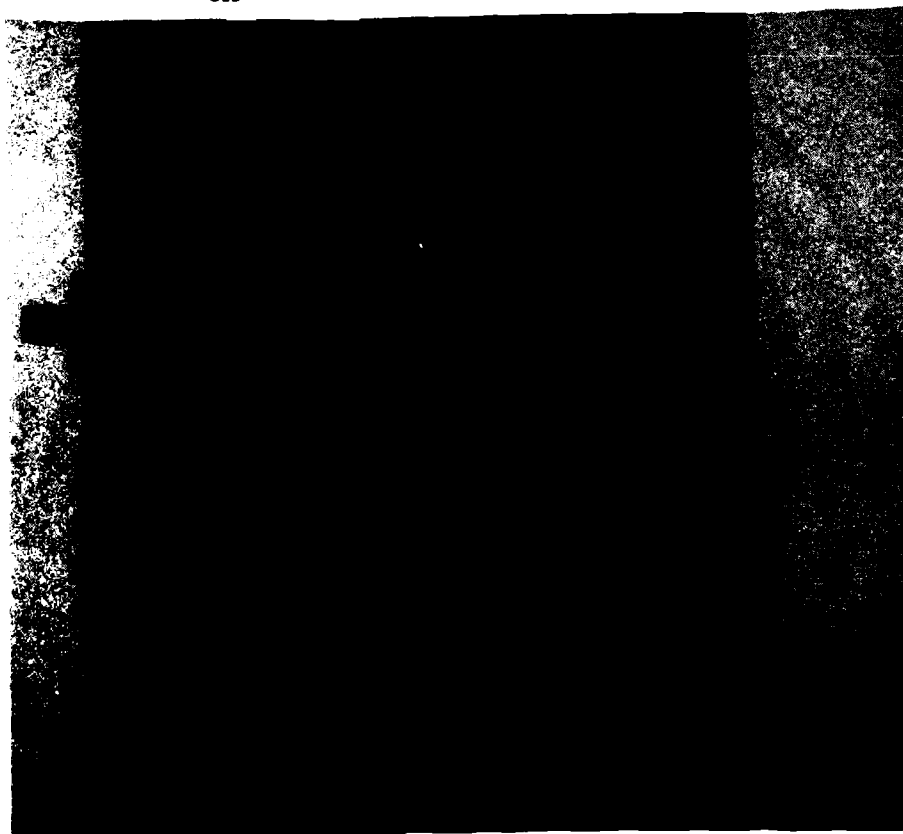


Figure 6. Photograph of the 6 GHz Patch Mounted in the Test Fixture

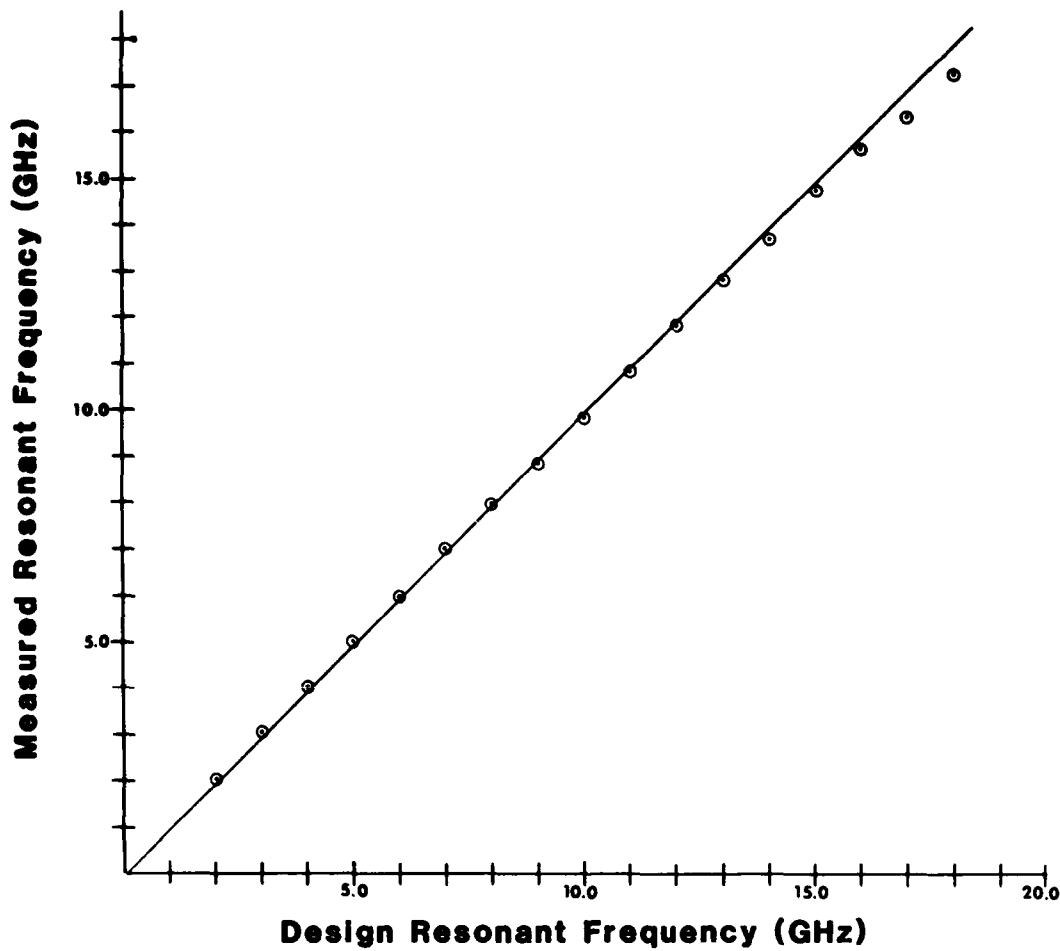


Figure 7. Measured Resonant Frequency vs. Design Frequency

The radiating slot is centered $\Delta l/2$ past the patch edge. We have modified our model to account for both of the above effects simply by using $l_1 = d\sqrt{\epsilon_{\text{eff}}} + \frac{\Delta l}{2}$ and $l_2 = (b-d)\sqrt{\epsilon_{\text{eff}}} + \frac{\Delta l}{2}$ in equation 11. Figure 8 shows the resonant frequency versus patch length for the original model, the modified model, and the measured data. The new model is very accurate at all frequencies.

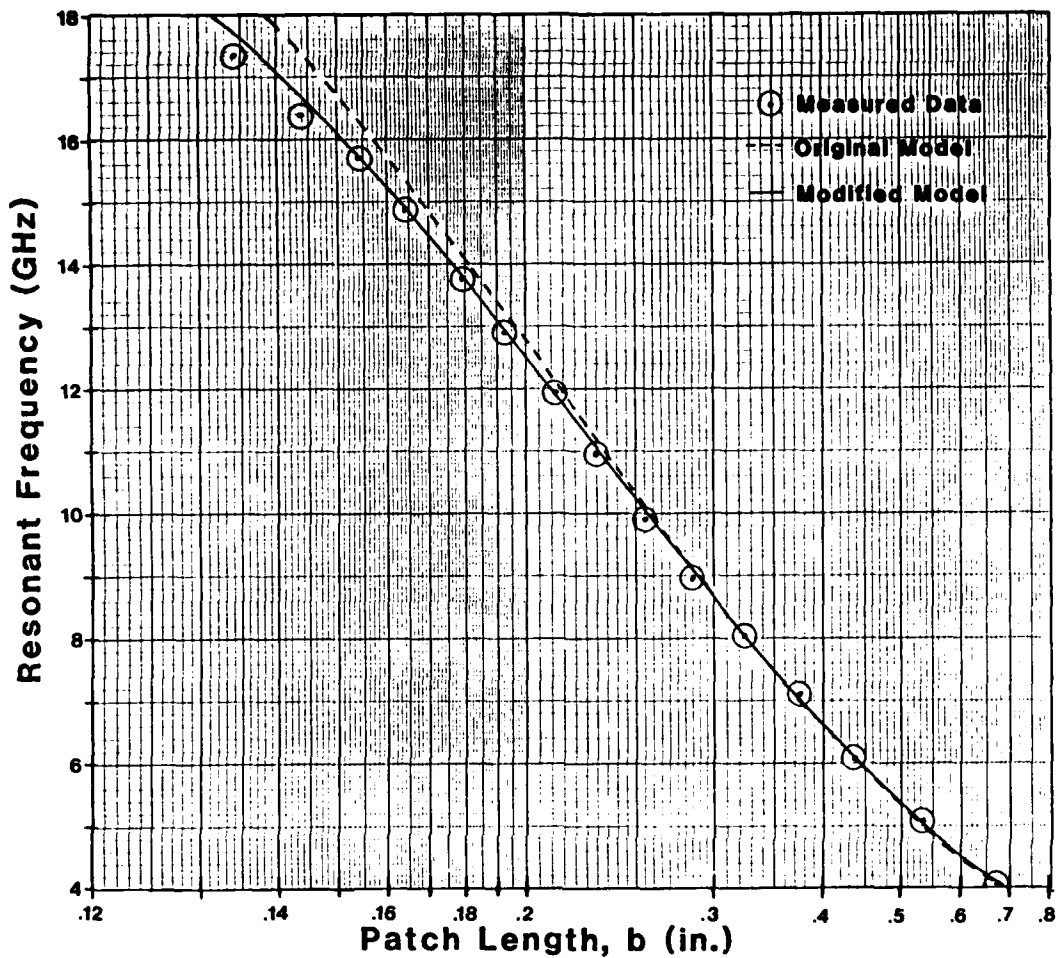


Figure 8. Resonant Frequency vs. Patch Length for Measured Data and Original and Modified Transmission Line Models

3.2 Return Loss

Just as the resonant frequency measurement is a direct test of the model's accuracy in predicting the patch length, b , the return loss measurement tests its accuracy in determining the feed point, or the dimension d . A sample return loss measurement for one of the antennas (6 GHz) is shown in Figure 9. To this measured return loss, we must add the two-way attenuation in the microstrip line between the network analyzer test port and the antenna's feed point, since that attenuation will tend to make the antenna's reflection coefficient appear smaller than it actually is. Figure 10 shows the loss per inch that we measured in a microstrip transmission line constructed on the same epoxy-fiberglass material as the antennas. The two way path loss was measured by placing an

open-circuit or a short-circuit termination at the end of the line, and the figure shows both cases. Figure 11 shows the corrected return loss vs. measured frequency for each of the 17 patches. All of the patches except two had very good return loss, which indicates that the depth of the inset feed corresponded to a close impedance match with the 100Ω feed line. The poor return loss of the 15 GHz and 17 GHz antennas was caused by delamination of the copper conductor from the substrate at the board edge due to repeated soldering and desoldering.

We recently constructed a rectangular patch antenna for 8 GHz using a probe feed, using the same transmission line model, except that both slots were considered to be of length a . The inset d was calculated for an impedance match to the 50Ω coax probe. The resonant frequency was 7.95 GHz, but the return loss at resonance was only -12 dB. This leads us to suspect that the failure of the transmission line model reported by other authors was due only to the fact that it cannot model the coaxial probe feed (most patch antenna experiments reported in the literature have used probe feeds).

3.3 Radiation Patterns

The E and H plane patterns of the 8 GHz antenna shown in Figures 12a and 12b are typical of those measurements. There is some irregularity in the E plane because of the edge-launch connector. Appendix A contains measured patterns up to 12 GHz, which is the limit of our anechoic chamber equipment.

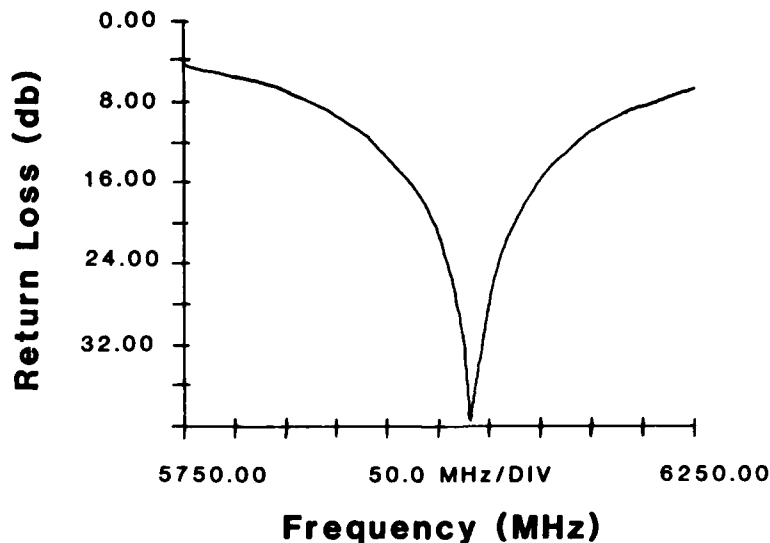


Figure 9. Typical Return Loss vs. Frequency (Measured)

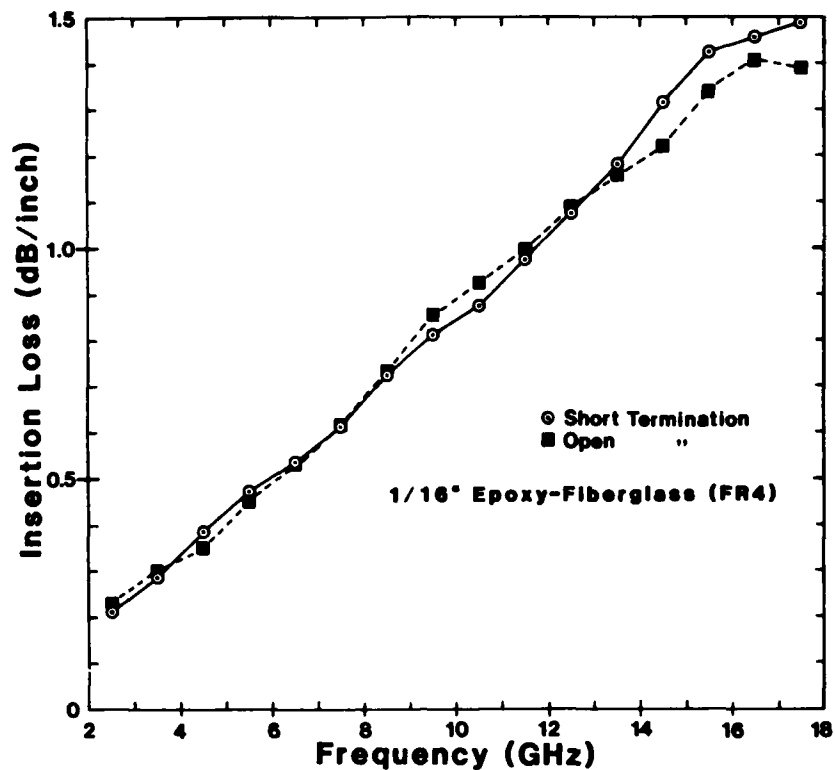


Figure 10. Measured Attenuation (db/inch) of a Microstripline on Epoxy

3.4 Bandwidth

The bandwidth for these individual patch antennas is calculated between 2:1 VSWR (10 dB return loss) points of the corrected (for line loss) measurement, and is shown in Figure 13. The increasing bandwidth with frequency is simply due to the increasing electrical thickness of the substrate, and is within the bounds we would expect from calculations by Bahl & Bhartia⁸. The extremely small bandwidth is an obvious disadvantage of microstrip antennas, but improvements in that area were not an objective of this project.

4. REACTIVE POWER DIVIDERS

The next step in our development of arrays was to design a coplanar feed network with microstrip power dividers. There is not enough room on the substrate for hybrid

8. Bahl, I.J. and Bhartia, P. (1981) Microstrip Antennas, Artech House.

or Wilkinson power dividers, so we chose a simple reactive design. Five power dividers with resonant frequencies of 2, 4, 8, 12 and 16 GHz were built and tested, one of which is shown in Figure 14. Unlike the patch antennas, these were etched on a PTFE substrate which has a 2.54 dielectric constant and low dielectric loss (1/16" thick Oak-602®).

The characteristic impedance of the microstrip lines in this power divider is 100Ω , and therefore, we must have the input and output transformers (70.7Ω) to match the three lines to the 50Ω coaxial connectors. The input line goes into a quarter-wavelength transformer whose impedance is also 70.7Ω , which matches the input line to the two output lines, whose parallel impedance is 50Ω . Since both output ports have the same impedance, this is an equal split power divider.

The length of the transformers, both at the connectors and in the main arm of the power dividers, is one quarter of a guide wavelength. The fields of a microstrip line

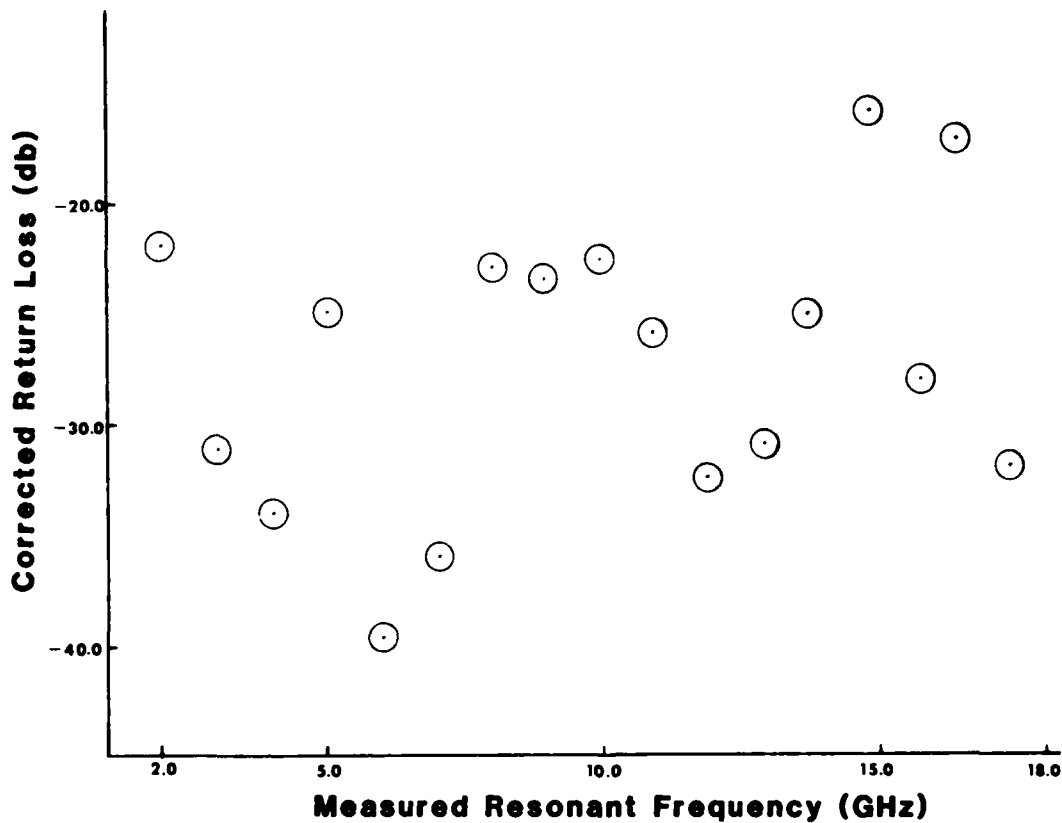


Figure 11. Return Loss of the Experimental Patch Antennas

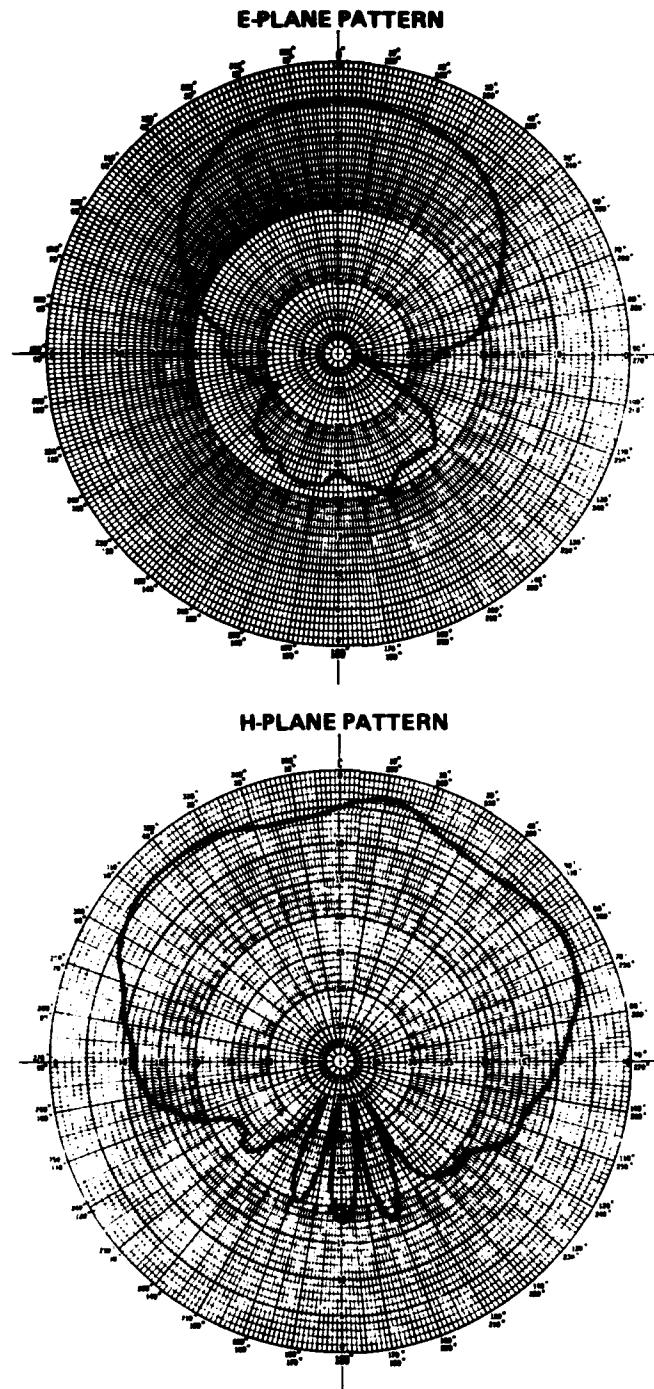


Figure 12. Typical Radiation Patterns (8 GHz Patch): (a) E Plane, (b) H Plane

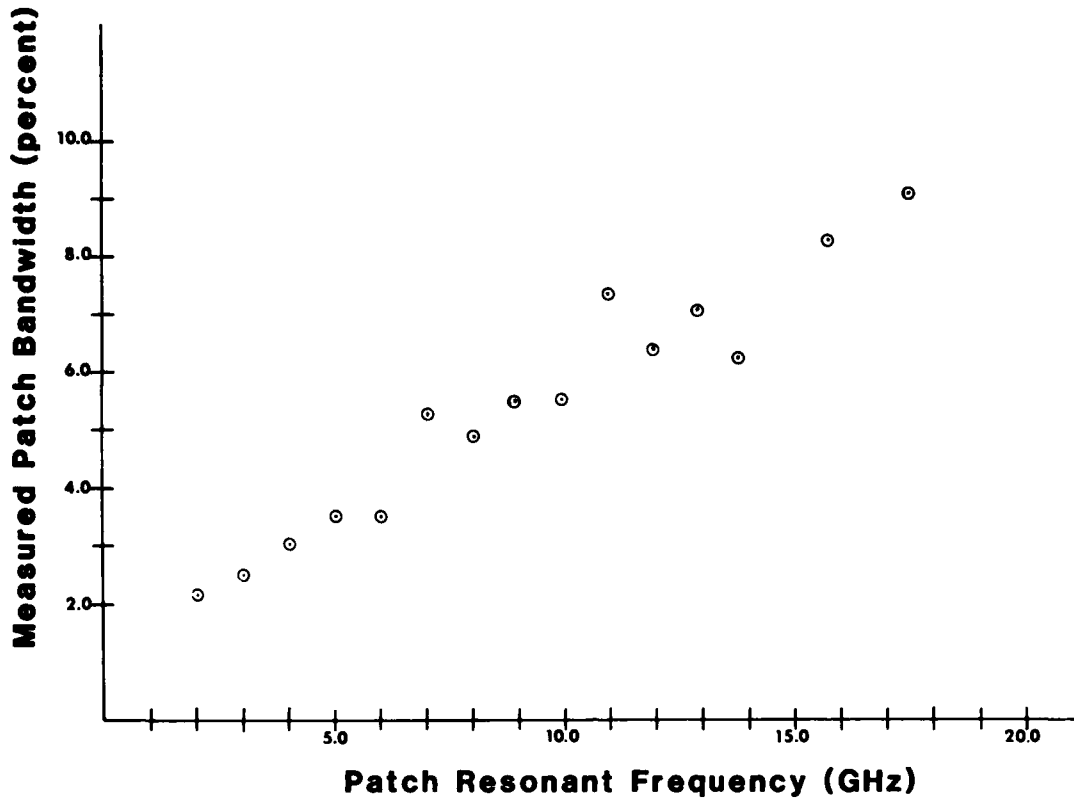


Figure 13. Measured Bandwidth of the Experimental Patch Antennas

pass through both air and dielectric, as illustrated in Figure 15, which changes the effective dielectric constant and hence also the guide wavelength. The structure of those fringing fields changes with frequency, and therefore so does the effective dielectric constant and the velocity of propagation. In the power divider design it is important to find the correct length for the transformer sections so that reflections are minimized at the design frequency. The guide wavelength is calculated as $\lambda_g = \lambda_0 / \sqrt{\epsilon_{eff}}$, where⁴:

$$\epsilon_{eff}(f) = \epsilon_r - (\epsilon_r - \epsilon_{eo}) / [1 + G(f/f_p)] \quad (13a)$$

$$\epsilon_{eo} = \frac{\epsilon_r + 1}{2} + \frac{\epsilon_r - 1}{2} (1 + 10h/w)^{-1/2} + \frac{\epsilon_r - 1}{4.6} \frac{t/h}{\sqrt{w/h}} \quad (13b)$$

$$G = \sqrt{(Z_0 - 5)/60} + .004Z_0 \quad (13c)$$

$$f_p = 15.66Z_0/h \times 10^6 \quad (13d)$$

where f is the frequency, Z_0 is the characteristic impedance of the transformer section, w is its width, h is the substrate thickness, and ϵ_r is its dielectric constant.

The corrected return loss for the three ports is given in Figure 16. It is the measured return loss minus the two-way line loss from the coaxial connector to the device and back. The return loss was high (corresponding to low VSWR) looking into the entry port, which we would expect since the device is impedance matched in that direction. It is not matched in the other direction, and therefore the output ports have low return loss, also shown in Figure 16.

An ideal two-way divider would have 3 dB insertion loss from the input to each of the outputs. Figure 17 shows that our outputs were well balanced. However, the insertion loss was typically higher than 3 dB, as shown in Figure 18, due to losses in the circuit. We would also like to have high isolation between the outputs (>20 dB), but our 6-10 dB is typical of this simplified design. Note that Figures 16, 17 and 18 show data for the actual measured resonant frequencies. Those were lower than the design

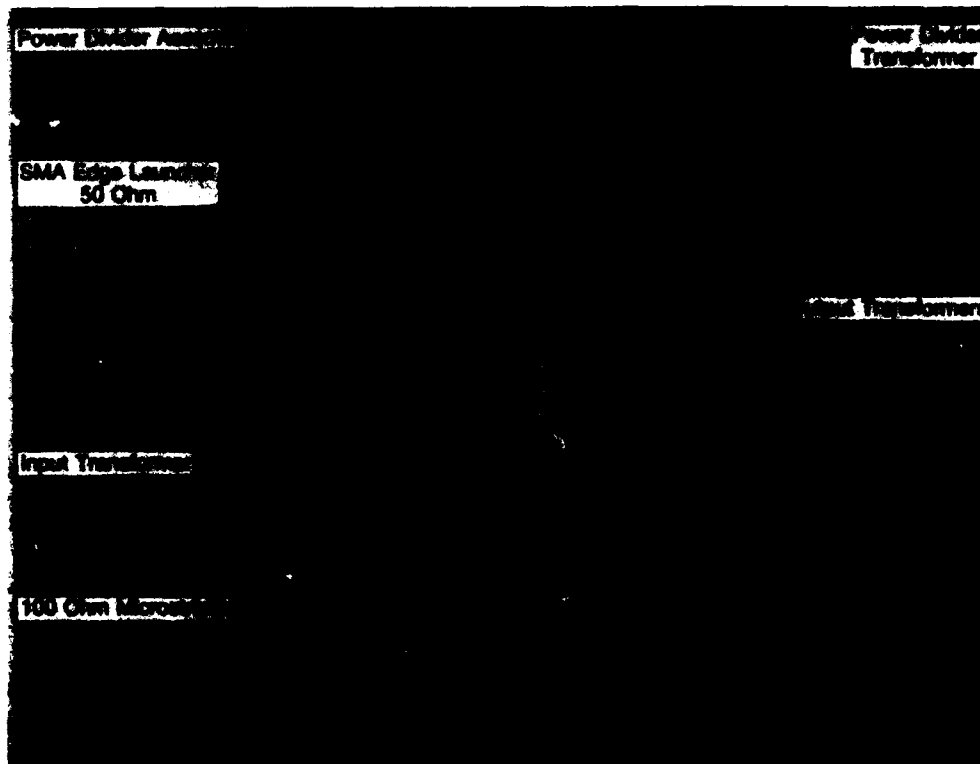


Figure 14. Power Divider Mounted in Test Fixture

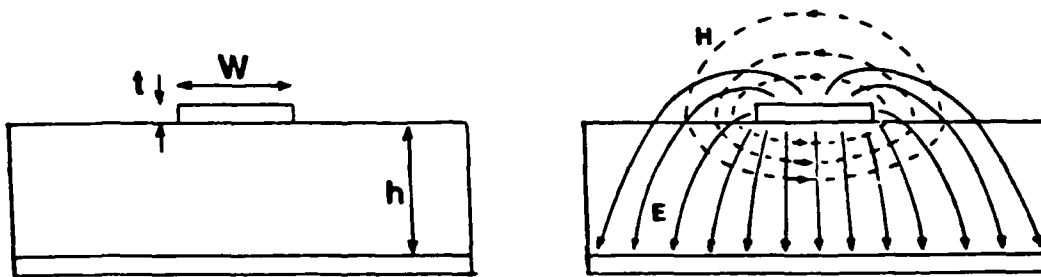


Figure 15. Fringing Fields of Microstrip Transmission Line

frequency because the two arcs that make up the output lines bled together on the artwork mask, making the actual transformer length greater than designed. As we will show later, this is avoided by mitering the two lines away from each other immediately past the transformer.

For comparison, we measured a 4.0 GHz equal-split Wilkinson divider built earlier by K. Huck². The Wilkinson design uses several transformer sections, plus an isolation resistor between the two output arms. Its isolation between the output ports was 9.8 dB, which is only slightly better than the 7 dB from our simplified 4 GHz divider. The Wilkinson's output ports, however, were very well impedance matched, with 21.6 dB, 20.3 dB and 21.4 dB return loss for, respectively, the input port, left exit and right exit. That advantage comes at the expense of higher overall loss, which was 1.39 dB. In any case, there is scarcely enough space on a typical printed circuit array for a feed network using simplified dividers, let alone Wilkinsons, in practical microstrip arrays.

5. PATCH ARRAY WITH INTEGRAL CORPORATE FEED

The 16-element array shown in Figure 19 was a test of the effectiveness of our computer-aided design system in providing accurate printed circuit antennas. The substrate material is PTFE ($\epsilon_r = 2.54$, $h = .062$ "). It proved quite difficult to lay out an array on a material with such a low dielectric constant because the elements are physically large, leaving little room for the feed lines and power dividers. This array has $.75\lambda$ inter-element spacing, which allowed just enough room for the corporate feed, observing the general rule of thumb that the transmission lines should not come within 3 board thicknesses of any patch or any other line.

The measured return loss of the array is shown in Figure 20. The actual resonant frequency is 8.02 GHz, only .25% above the design frequency. The H plane pattern is shown in Figure 21. The very deep nulls in the pattern are an indication of low phase

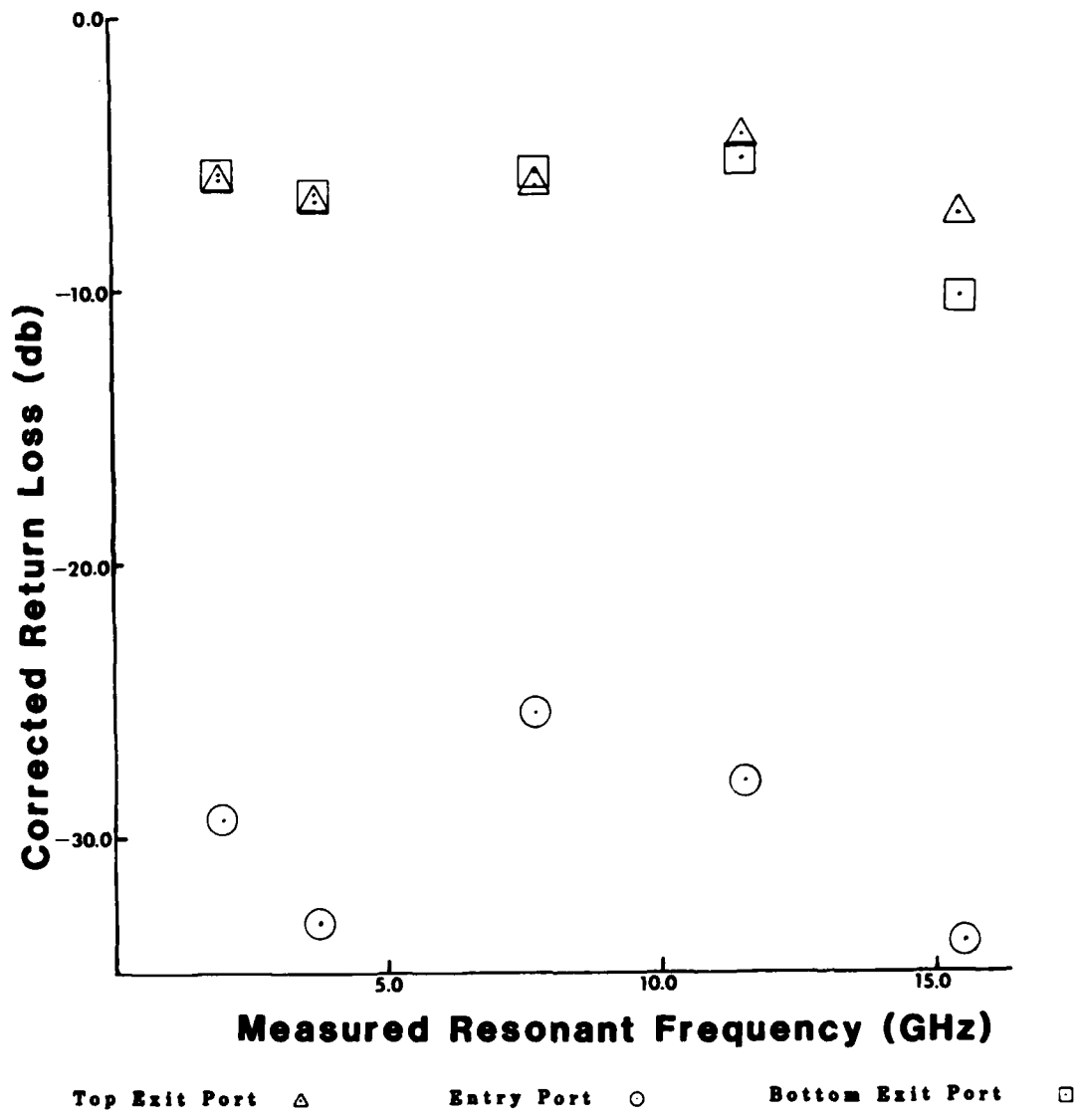


Figure 16. Return Loss of the Experimental Power Dividers at Input Port and Output Ports

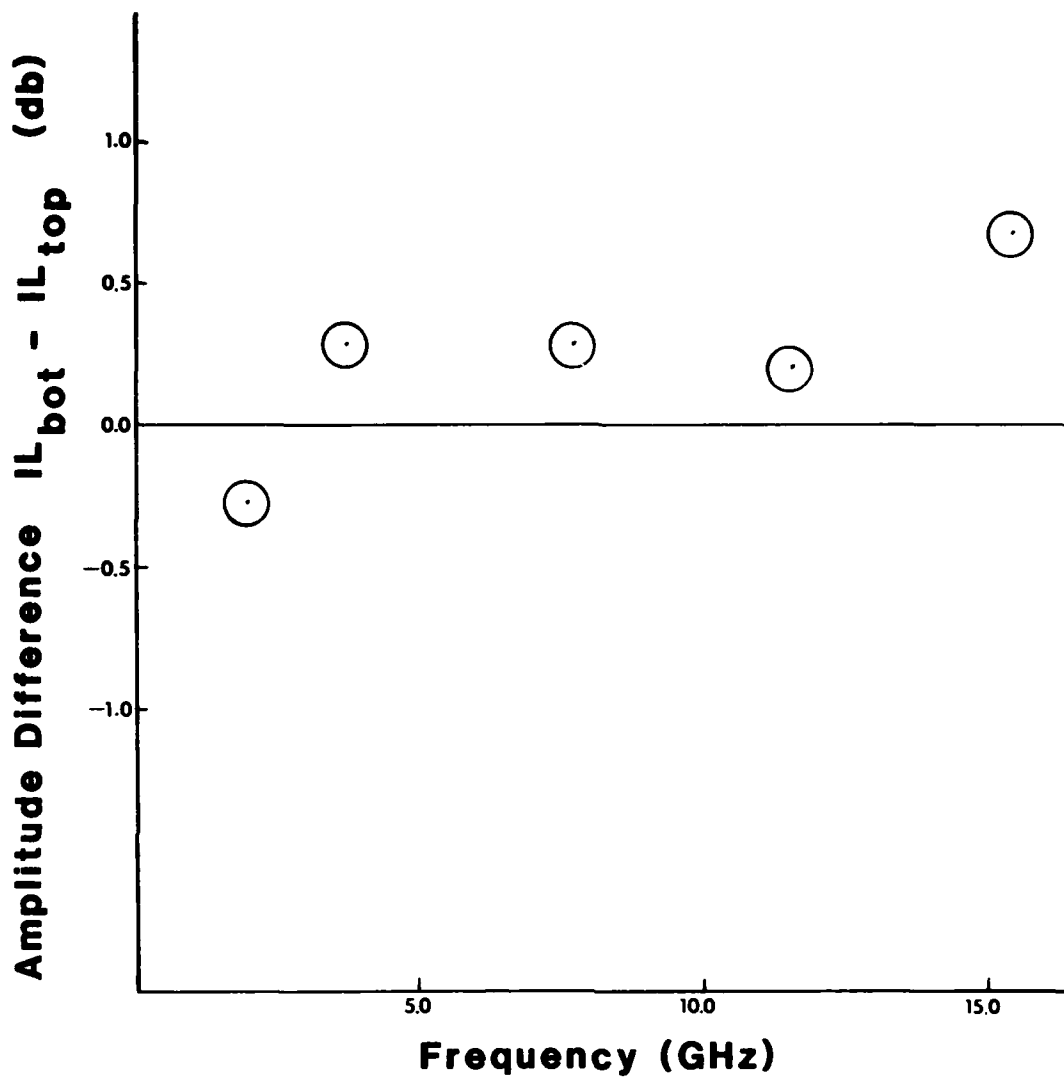


Figure 17. Amplitude Balance in the Experimental Power Dividers

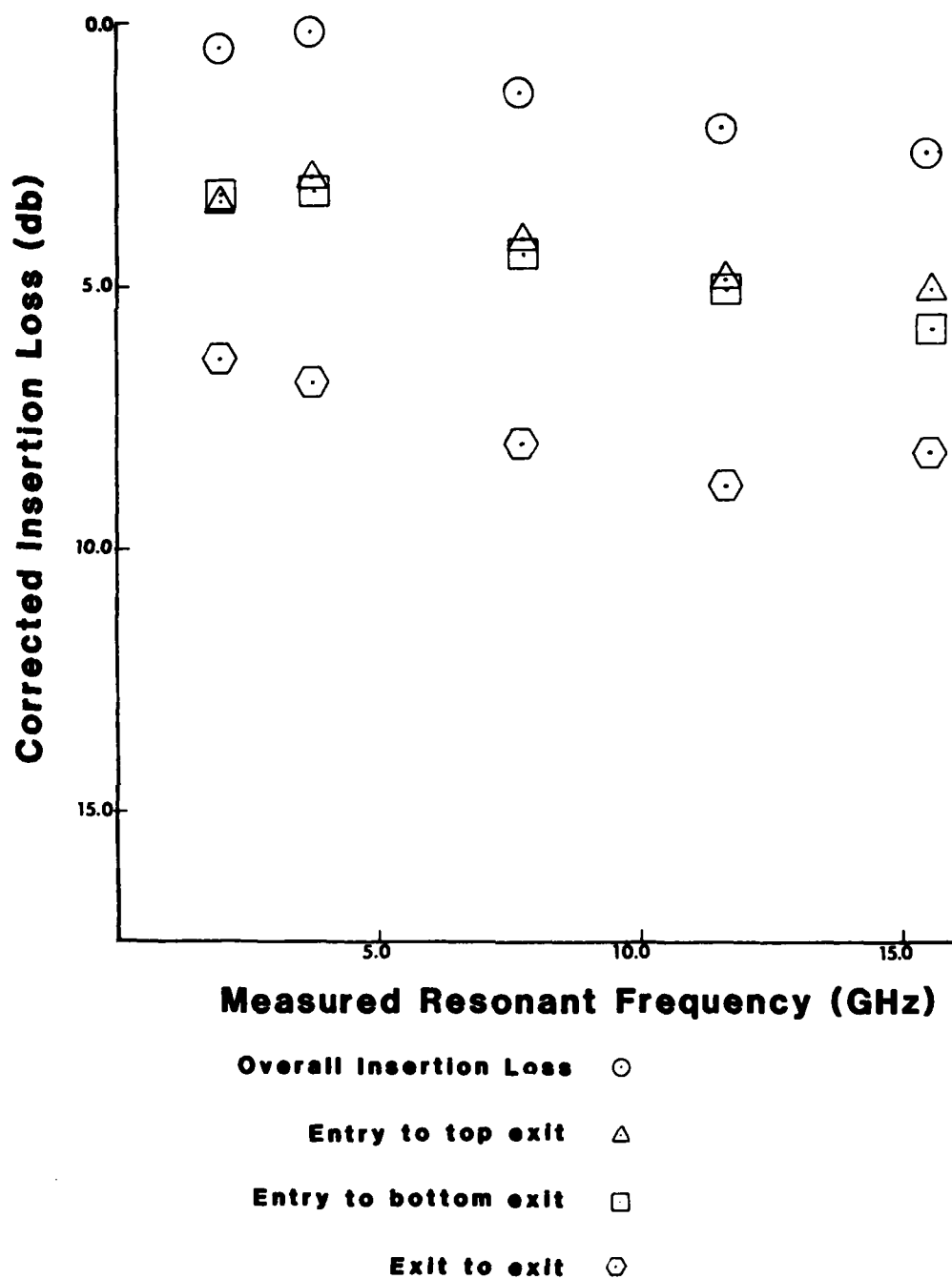


Figure 18. Insertion Loss, Net Power Loss and Isolation in the Experimental Power Dividers

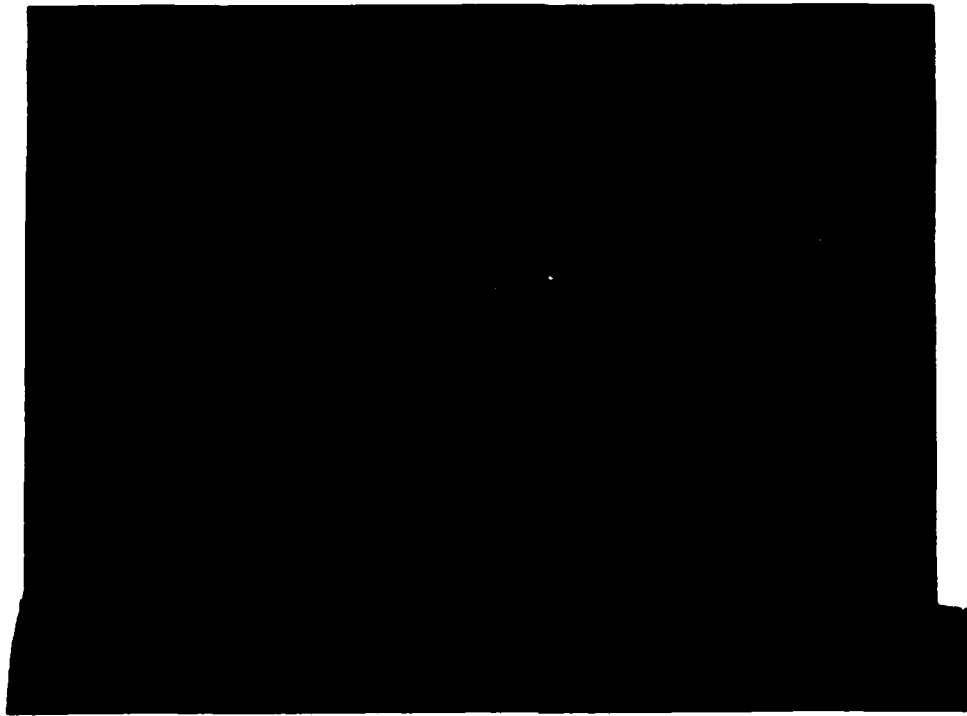


Figure 19. Microstrip Array Antenna with Integral Corporate Feed (8 GHz, $\epsilon_r=2.55$, $h=1/16''$)

error in the feed network. Due to the wide interelement spacing, the first sidelobes should be down 11.37 dB from the main beam peak, and they are very close to that (-11.5 dB and -12.2 dB), which is an indication of low amplitude error in the feed network. From this pattern we conclude that the corporate feed network's performance is very nearly ideal in distributing power to the 16 array elements with equal amplitude and phase.

The gain measurement shows that the array is quite efficient: the theoretical gain is 20.3 dB and the measured gain was 17.8 dB, or a net loss of 2.5 dB. Based on the measurements of transmission lines and power dividers discussed in the previous sections, we conclude that 1.6 dB of that loss is dielectric and conductor loss in the transmission lines, and .9 dB is residual loss in the power dividers.

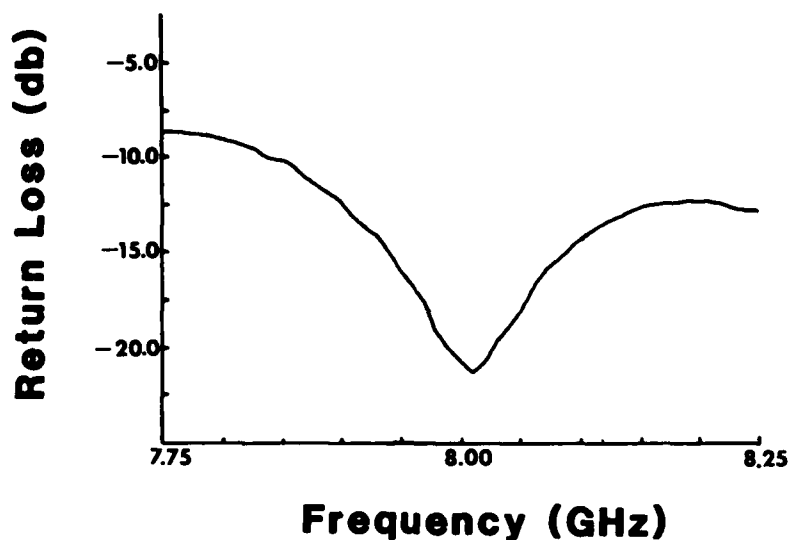


Figure 20. Measured Return Loss of the Experimental 4x4 Array

6. CONCLUSIONS AND RECOMMENDATIONS

In spite of its relative simplicity compared to other microstrip antenna models, the transmission line model has provided very accurate results, even for some cases in which the substrate is electrically thick. The model was within .5% of the resonant frequency in all cases except two when we used Hammerstad's approximation for the length extension to find the actual radiating slot location and the effective dielectric constant to find the propagation velocity within the patch. Since the materials to be used for monolithic millimeter wave antennas are electrically thin ($\sim .02 \lambda$) the transmission line model should accurately predict the resonant frequency and input impedance of a rectangular patch antenna on those substrates. We recommend some further experimentation with single patch antennas on a high dielectric constant material for purposes of verifying that conclusion, and to provide further data for refinements to our model.

An added attraction to the transmission line model is its possible application to other antenna geometries such as the "stagger-tuned" patch shown in Figure 22a. It might be modeled as five radiating slots and three transmission line sections as illustrated in Figure 22b. Extending the general analysis even further, one might be able to model any arbitrary geometry as a series of short transmission line sections and small radiating slots as shown in Figure 23.

The reactive power divider design we investigated was near-ideal in minimizing the input VSWR and in providing equal phase and amplitude between the two outputs. Unlike

Wilkinson power dividers and hybrids, it does not take up very much room on the substrate. Those qualities make it ideal for array applications such as our 16-element X-band antenna. That array also demonstrated the effectiveness of our computer-aided design package in quickly and accurately producing experimental hardware.

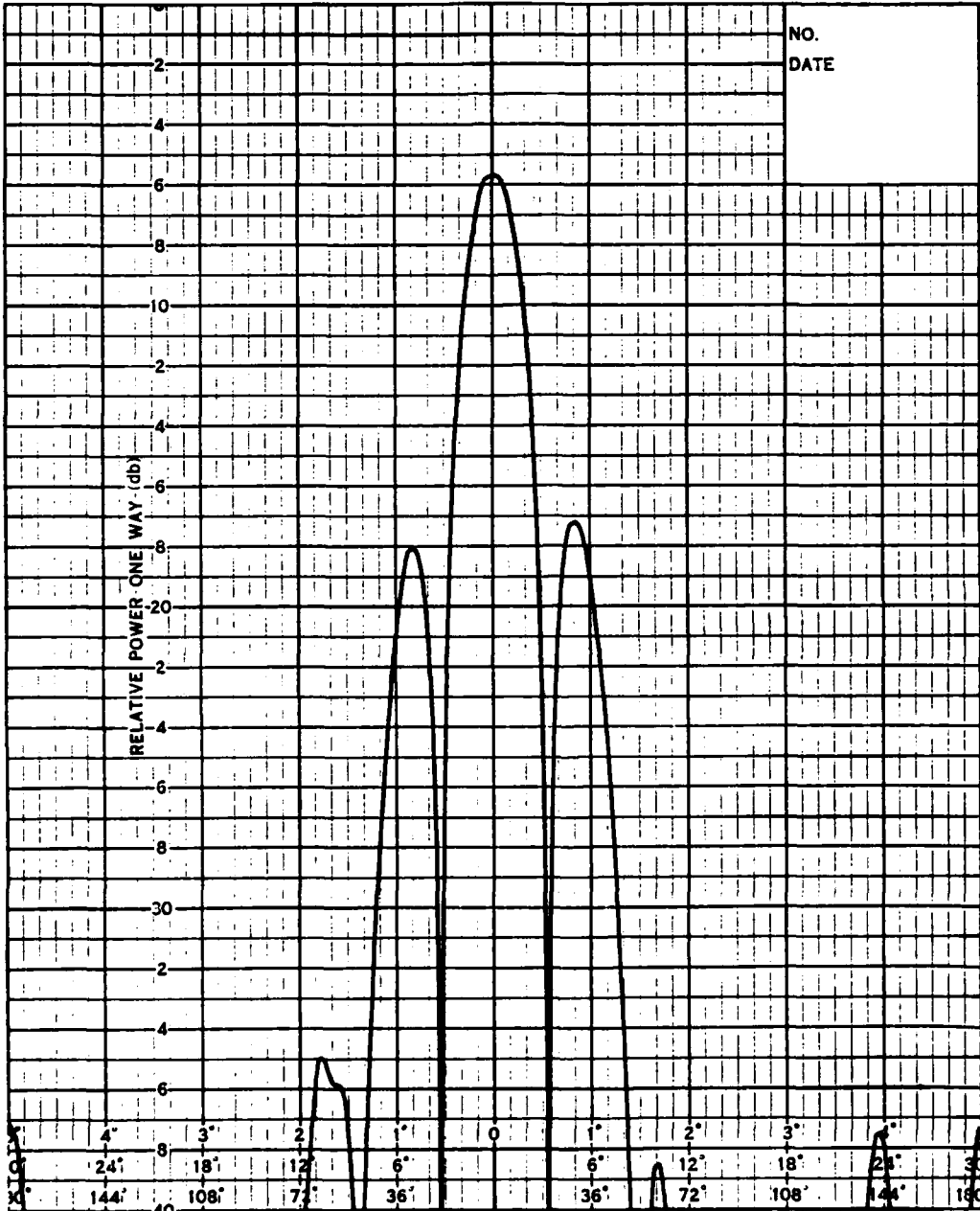


Figure 21. Measured E Plane Pattern of the Experimental 4x4 Array

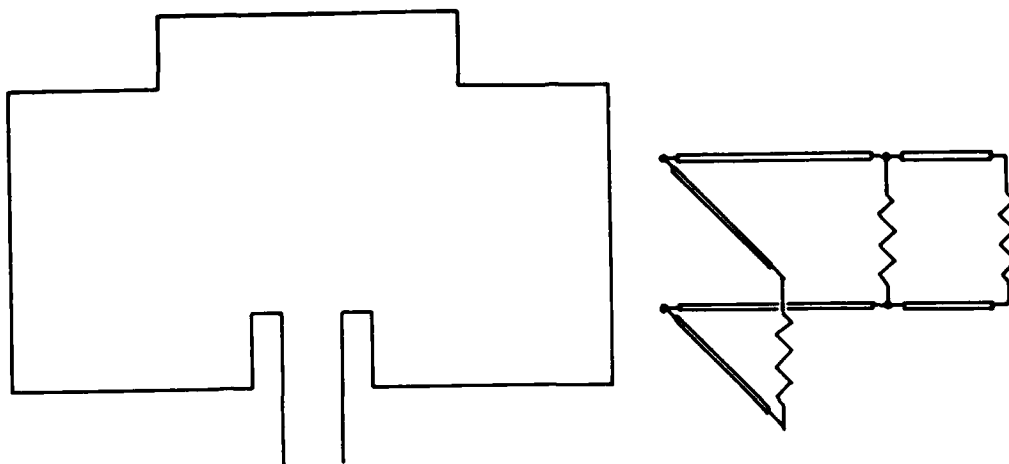


Figure 22. Stagger-Tuned Patch: (a) Geometry, (b) Model

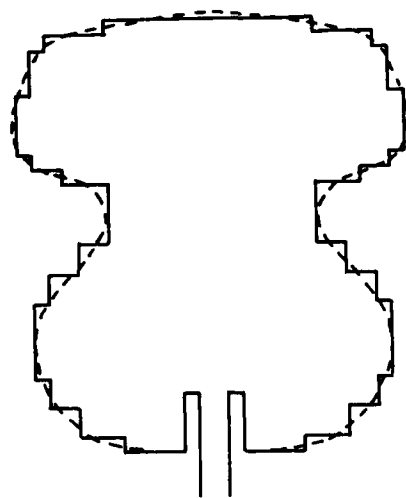


Figure 23. Arbitrary Patch Geometry

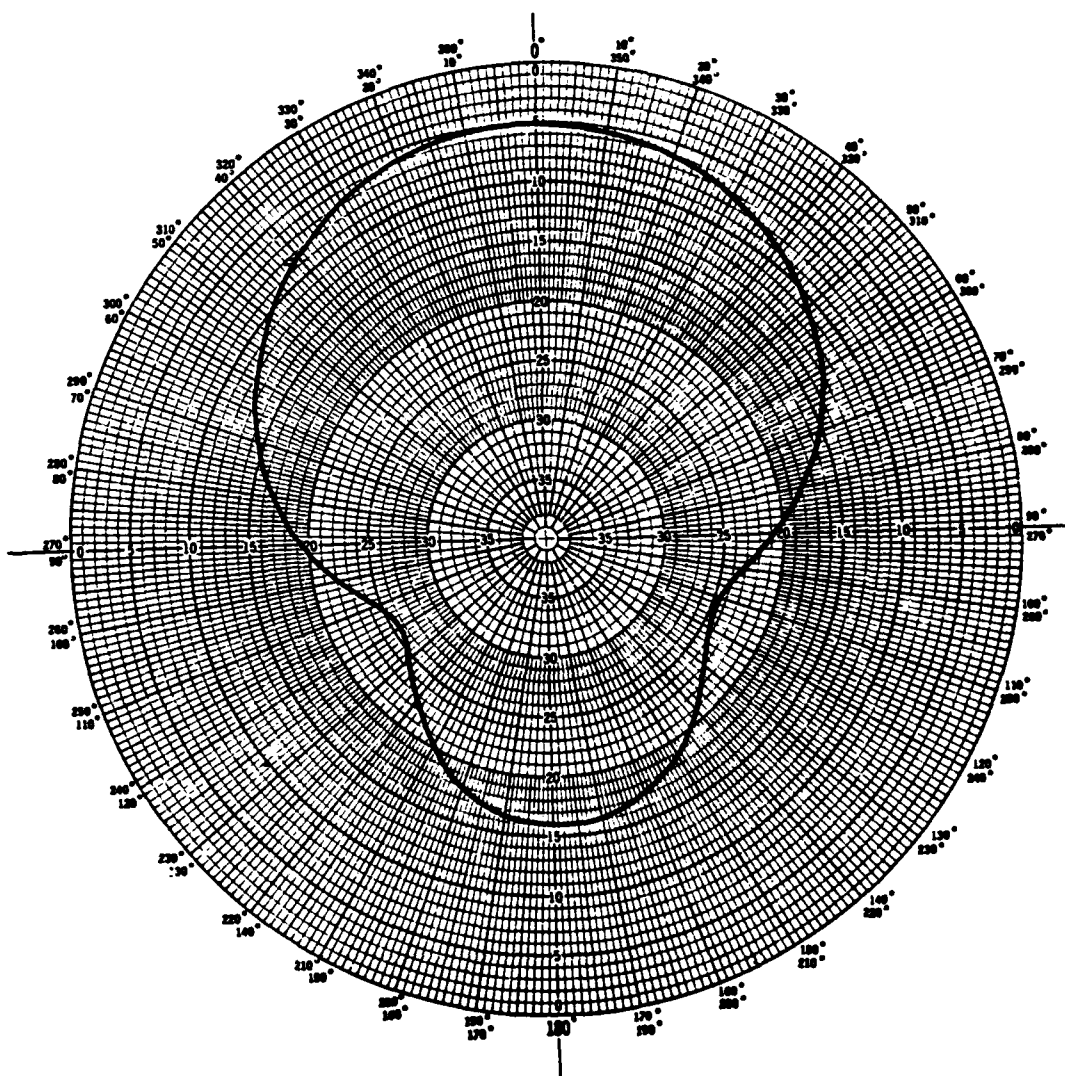
References

1. Kozak, F.E. and McGrath, D.T. (1985) Printed Circuit Transmission Line Transitions, RADC-TR-85-241, AD A169291.
2. Huck, K.D. (1986) Microstrip Amplitude-Weighted Wilkinson Power Dividers, RADC-TR-85-275, AD A169450.
3. Harrington, R.F. (1961) Time-Harmonic Electromagnetic Fields, McGraw-Hill.
4. Schaubert, D.H., Farrar, F.G., Sindoris, A. and Hayes, S.T. (1981) "Microstrip Antennas with Frequency Agility and Polarization Diversity," IEEE Transactions on Antennas and Propagation, AP-29, pp. 118-123.
5. Carver, K.R. and Mink, J.W. (1981) "Microstrip Antenna Technology," IEEE Transactions on Antennas and Propagation, AP-29, pp. 1-24.
6. Gupta, K.C., Garg, R. and Chadha, R. (1980) Computer Aided Design of Microwave Circuits, Artech House.
7. McGrath, D.T., Mullinix, D.A. and Huck, K.D. (1986) Fortran Subroutines for Design of Printed Circuit Antennas, RADC-TM-86-08.
8. Bahl, I.J. and Bhartia, P. (1981) Microstrip Antennas, Artech House.

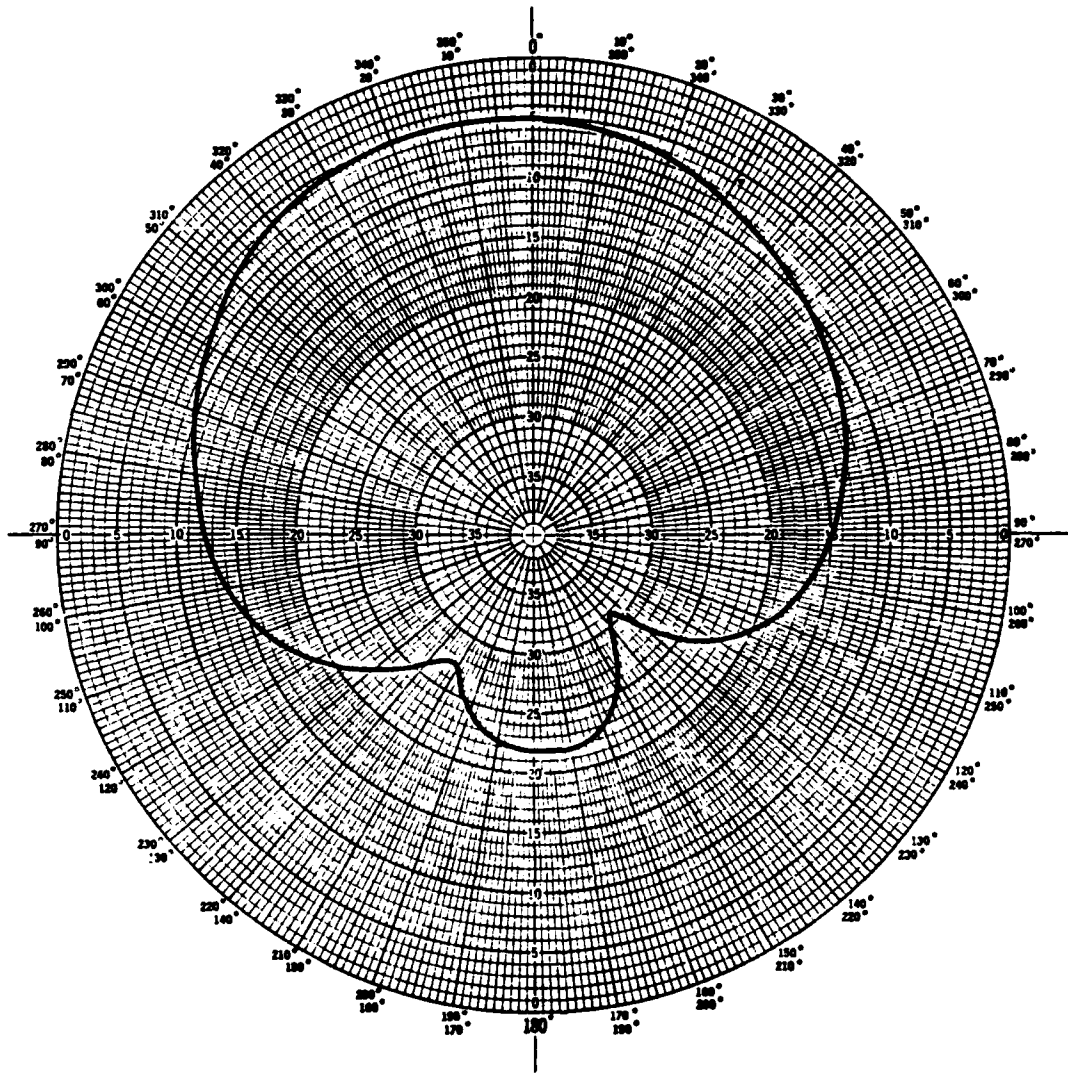
Appendix A

Patch Radiation Patterns

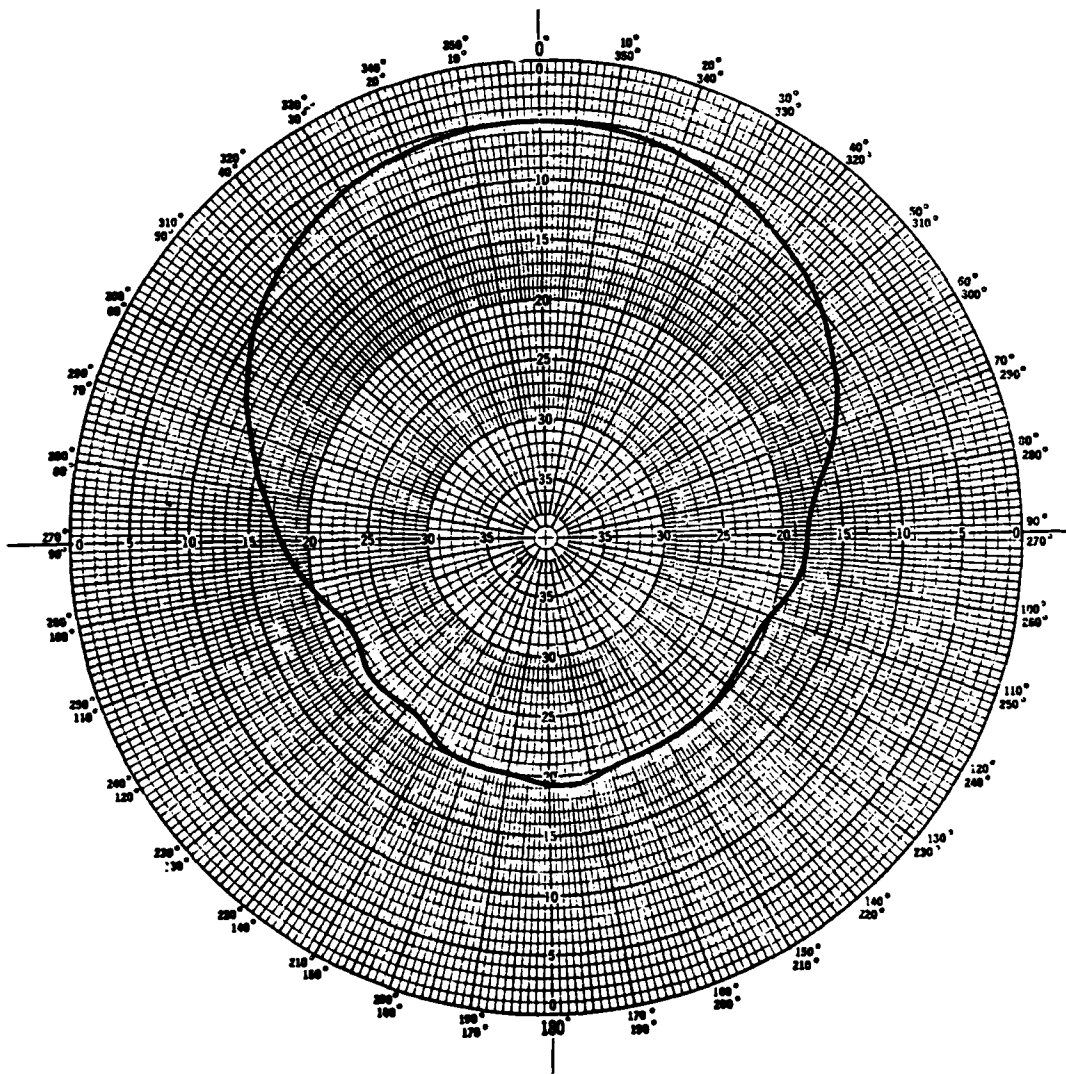
19 Feb 86
2.0 GHz Patch
H-Plane Pattern



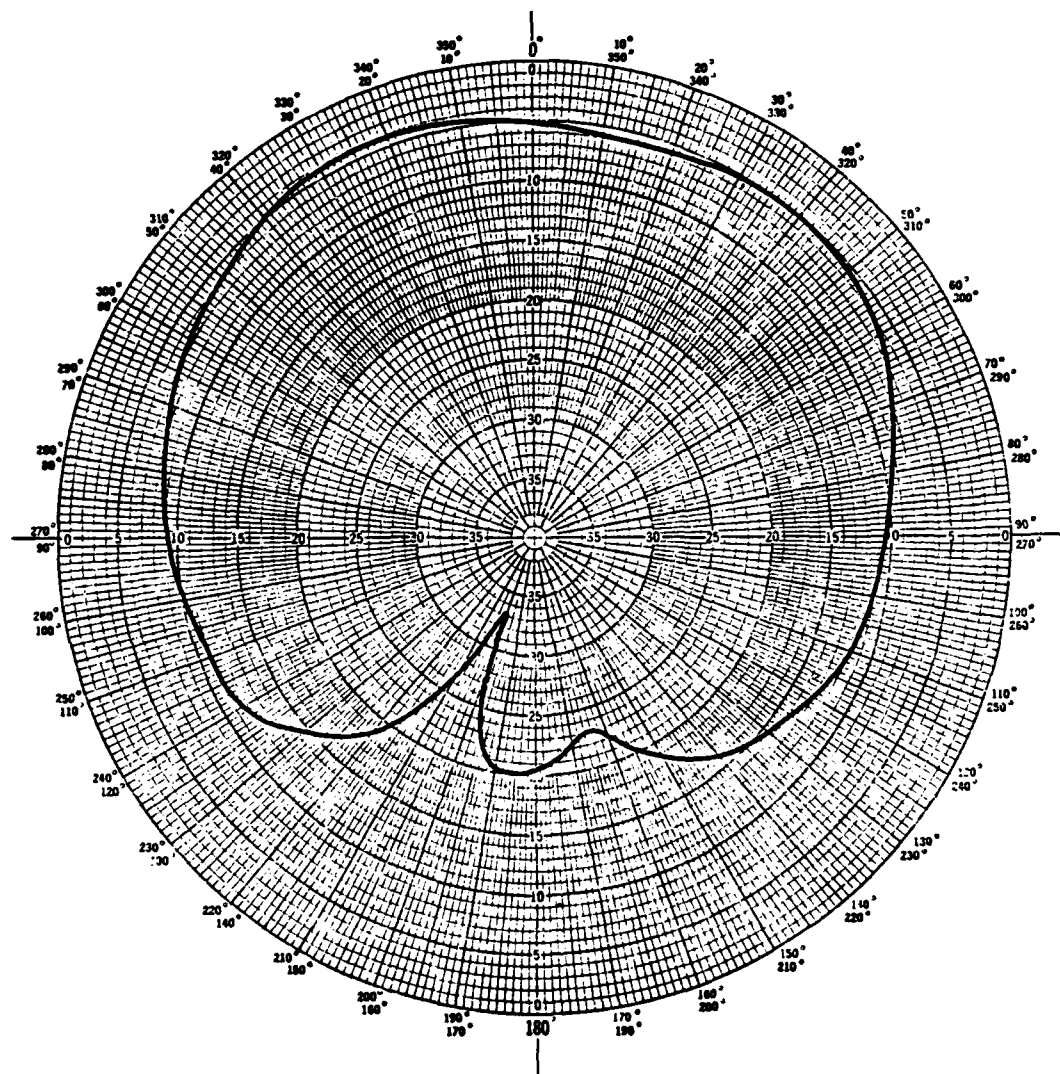
19 Feb 86
2.0 GHz Patch
E-Plane Pattern



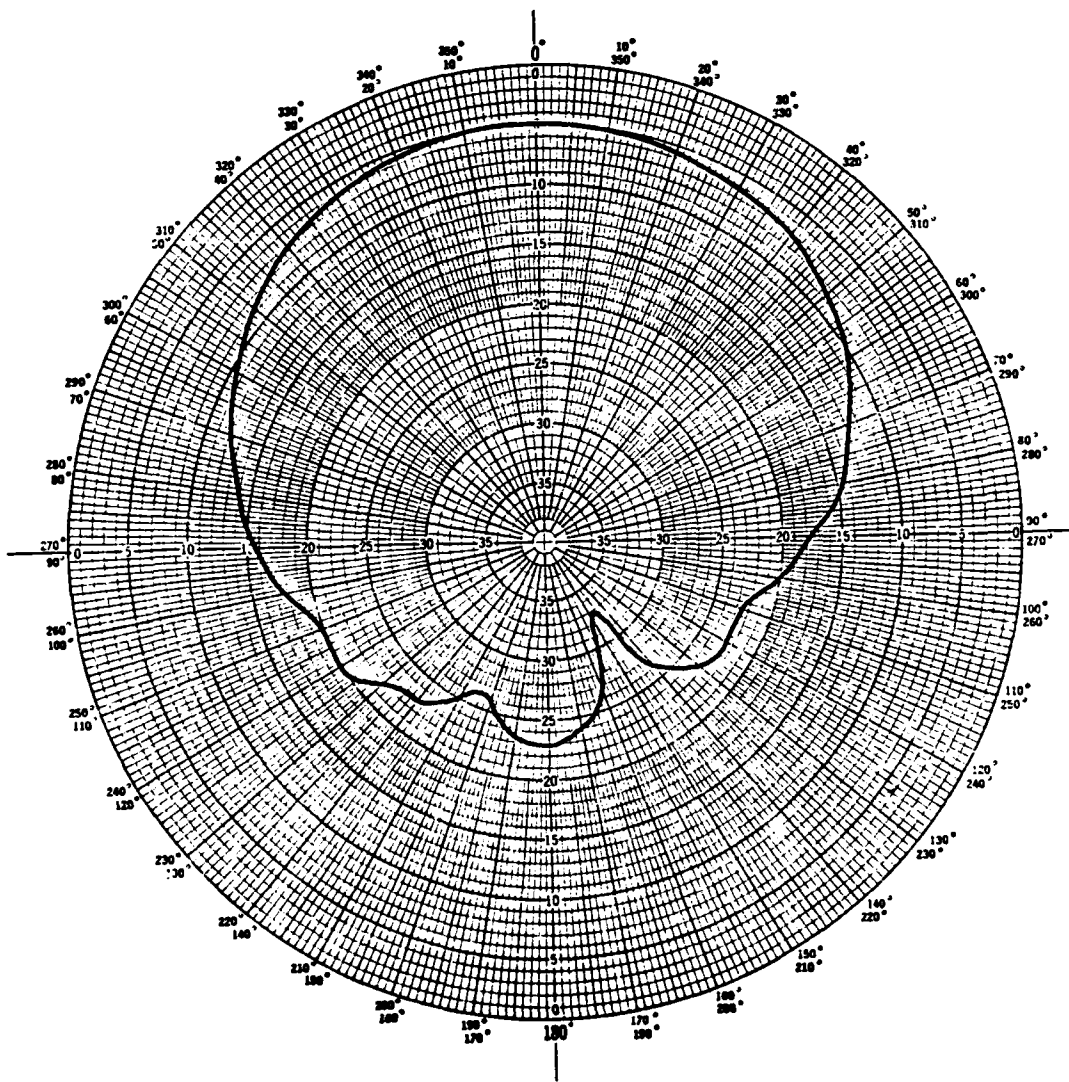
19 Feb 86
3.0 GHz Patch
H-Plane Pattern



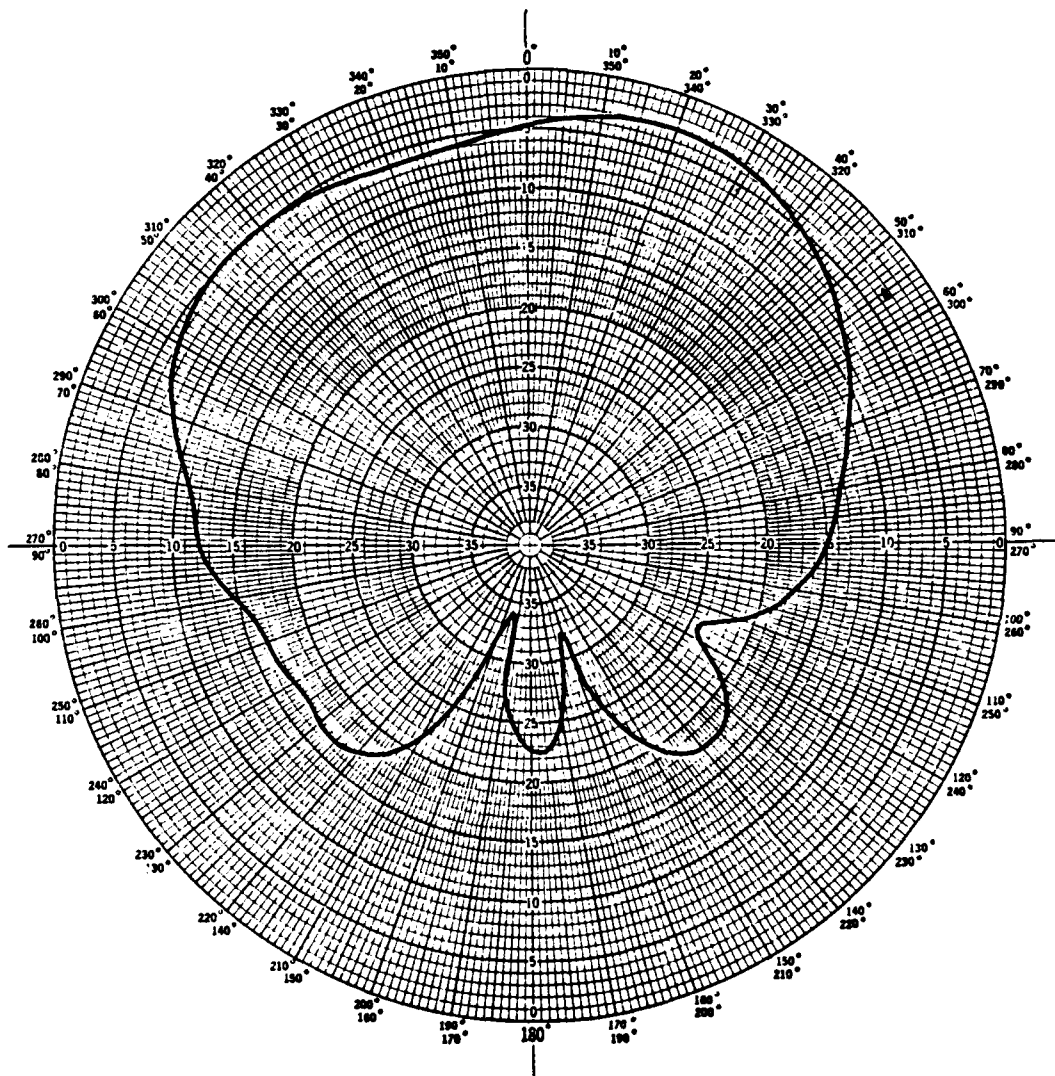
19 Feb 86
3.0 GHz Patch
E-Plane Pattern



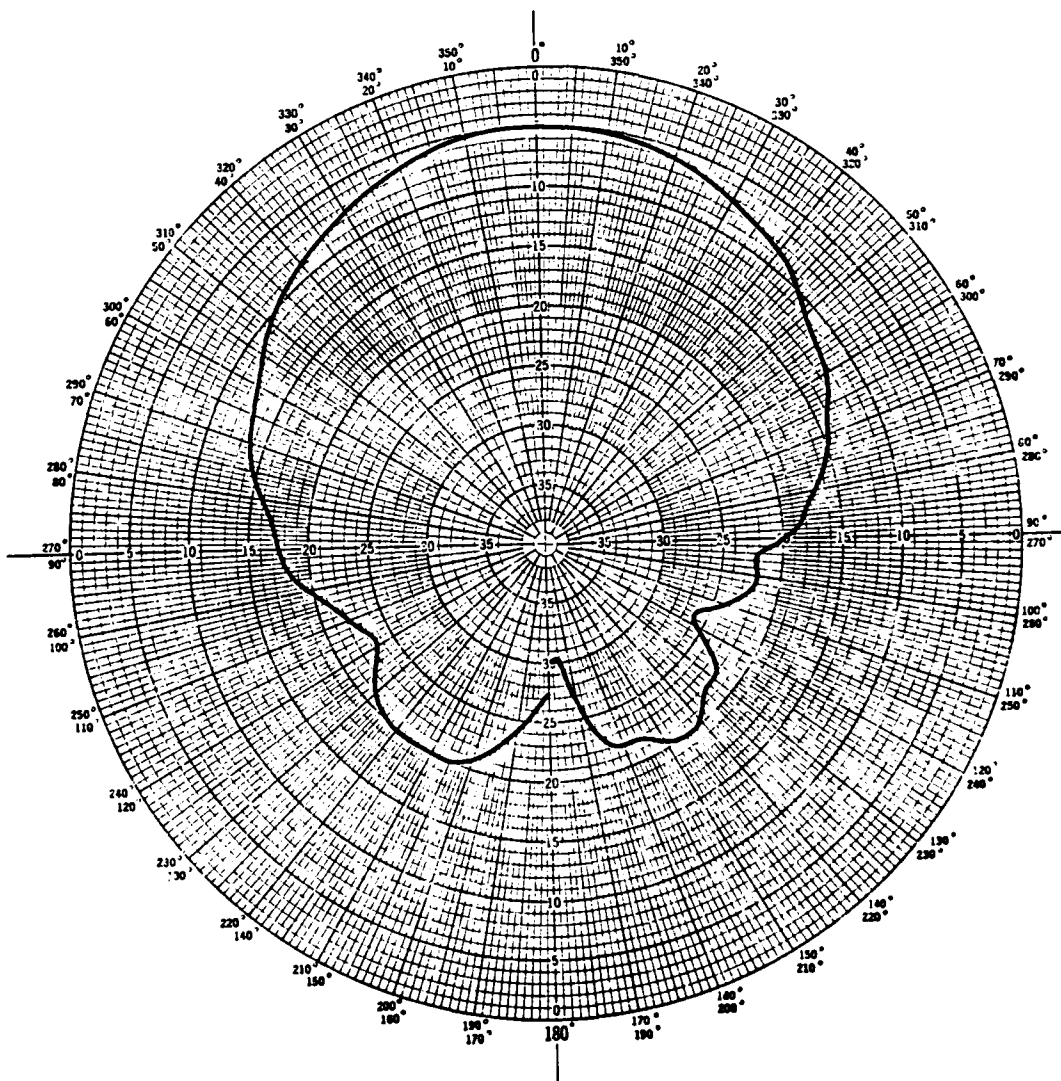
27 Jan 86
4.0 GHz Patch
H-Plane Pattern



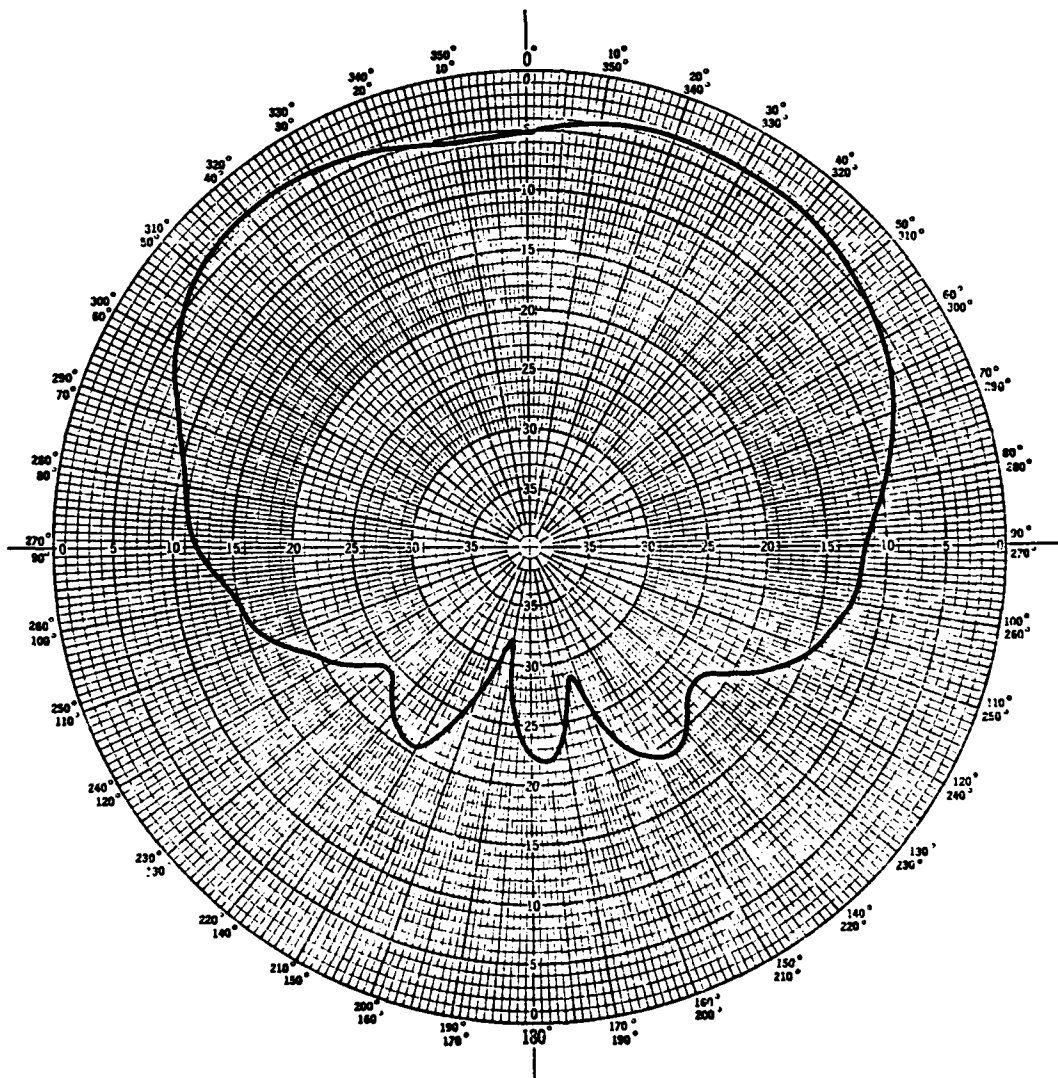
27 Jan 86
4.0 GHz Patch
E-Plane Pattern



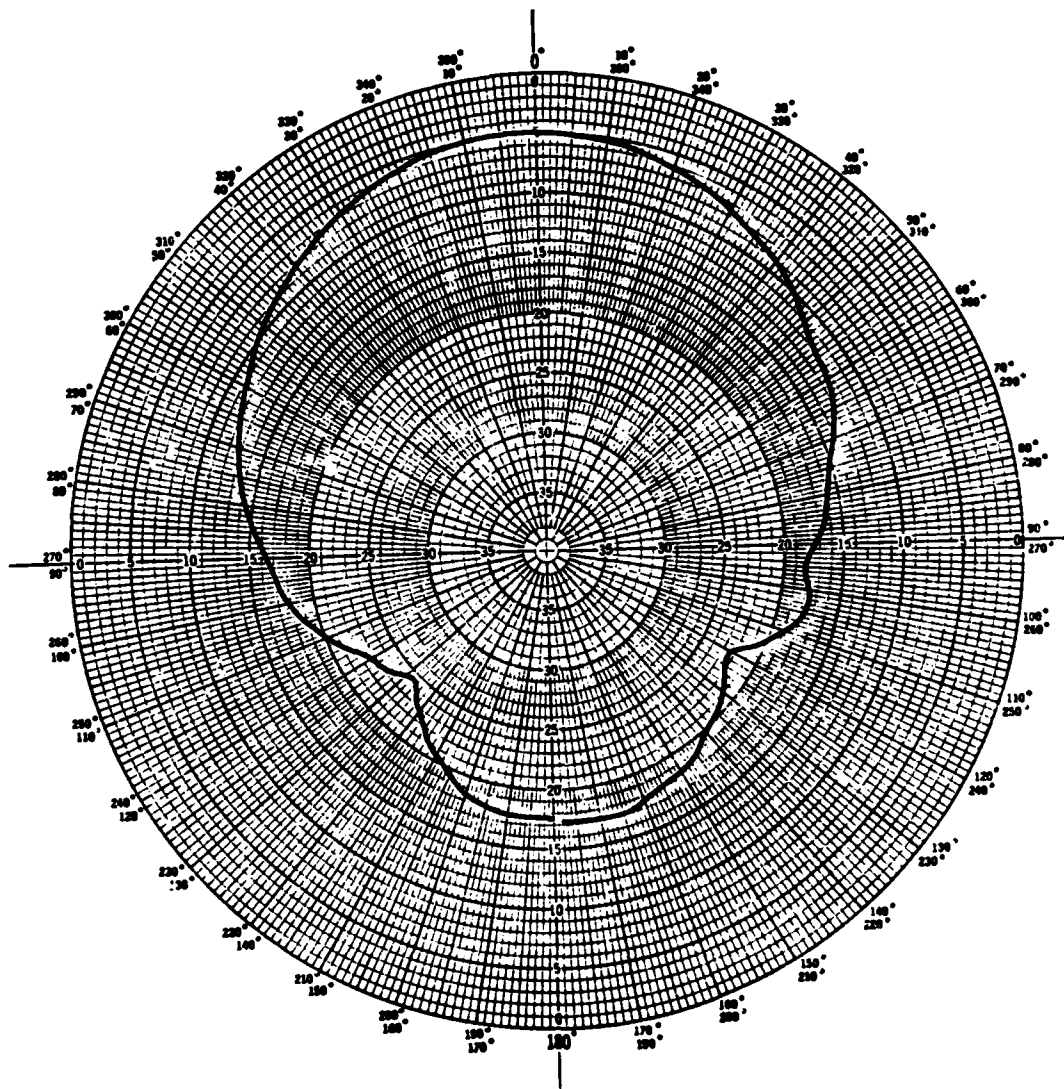
24 Jan 86
5.0 GHz Patch
H-Plane Pattern



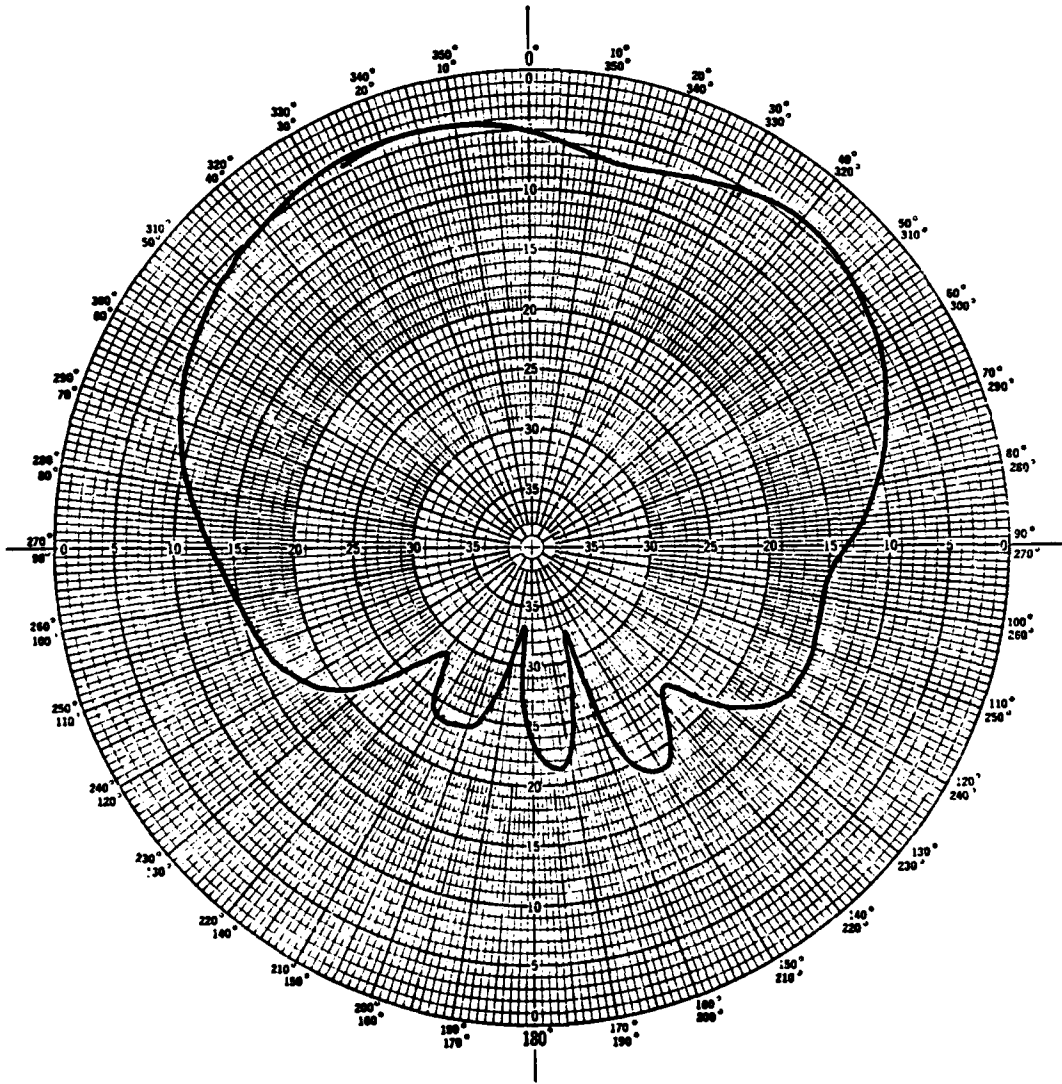
27 Jan 86
5.0 GHz Patch
E-Plane Pattern



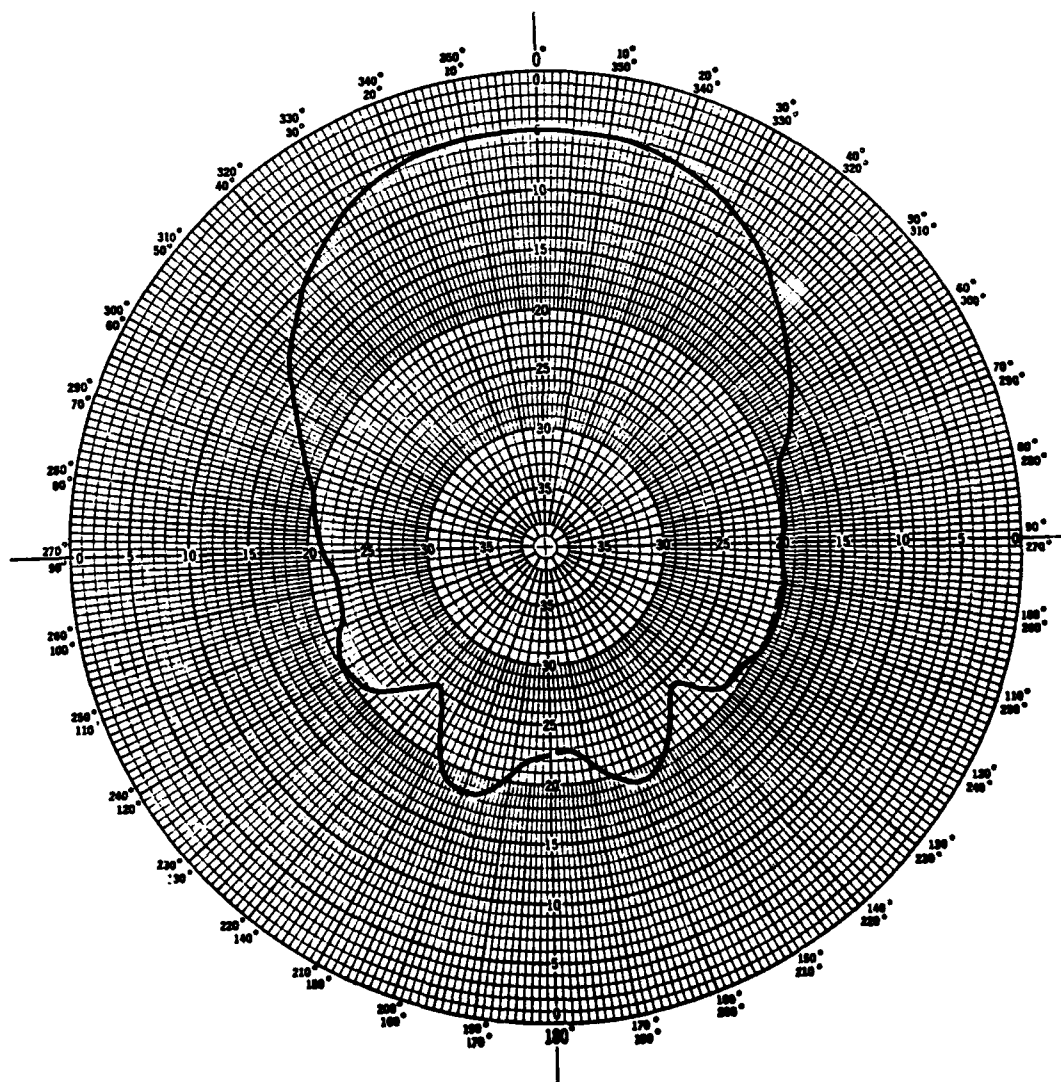
24 Jan 86
6.0 GHz Patch
H-Plane Pattern



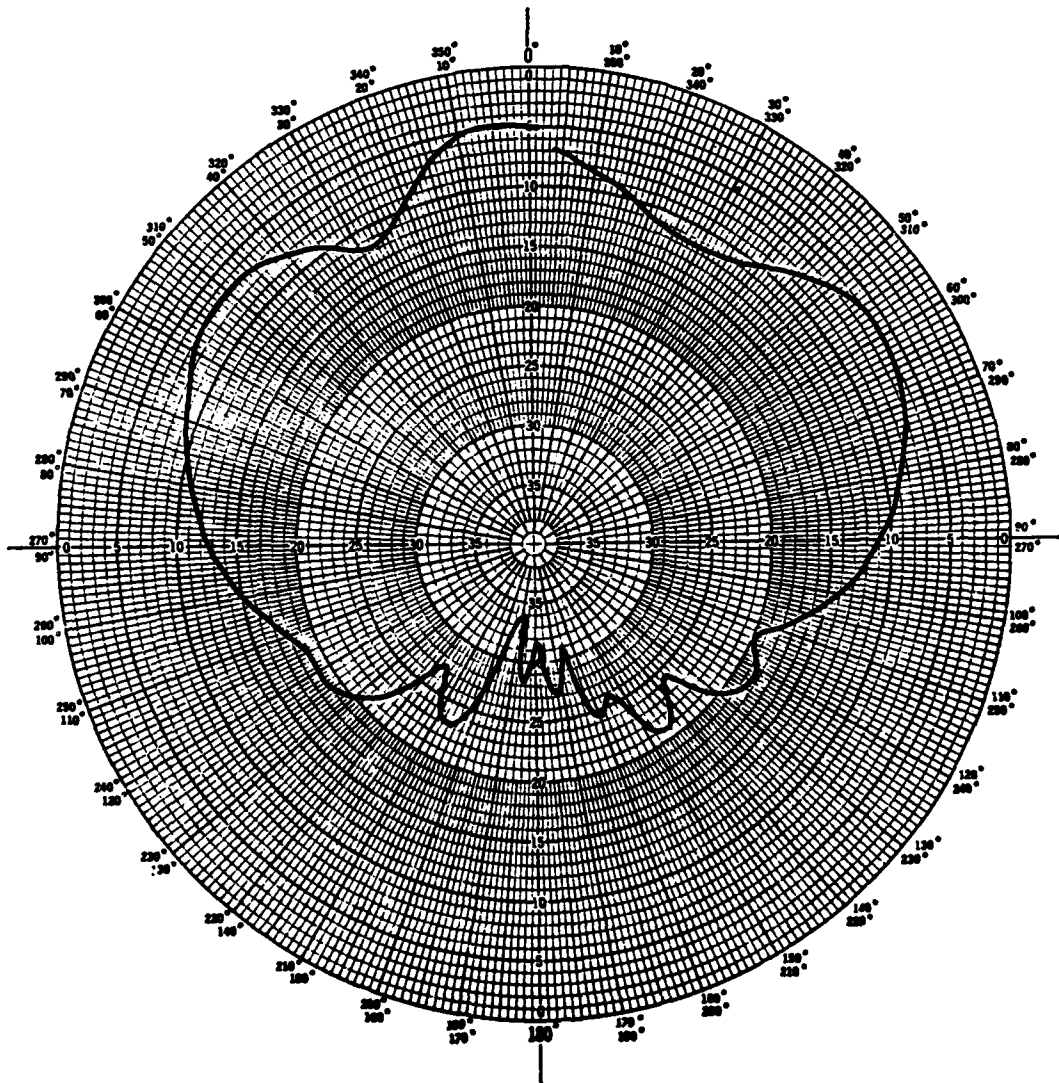
27 Jan 86
6.0 GHz Patch
E-Plane Pattern



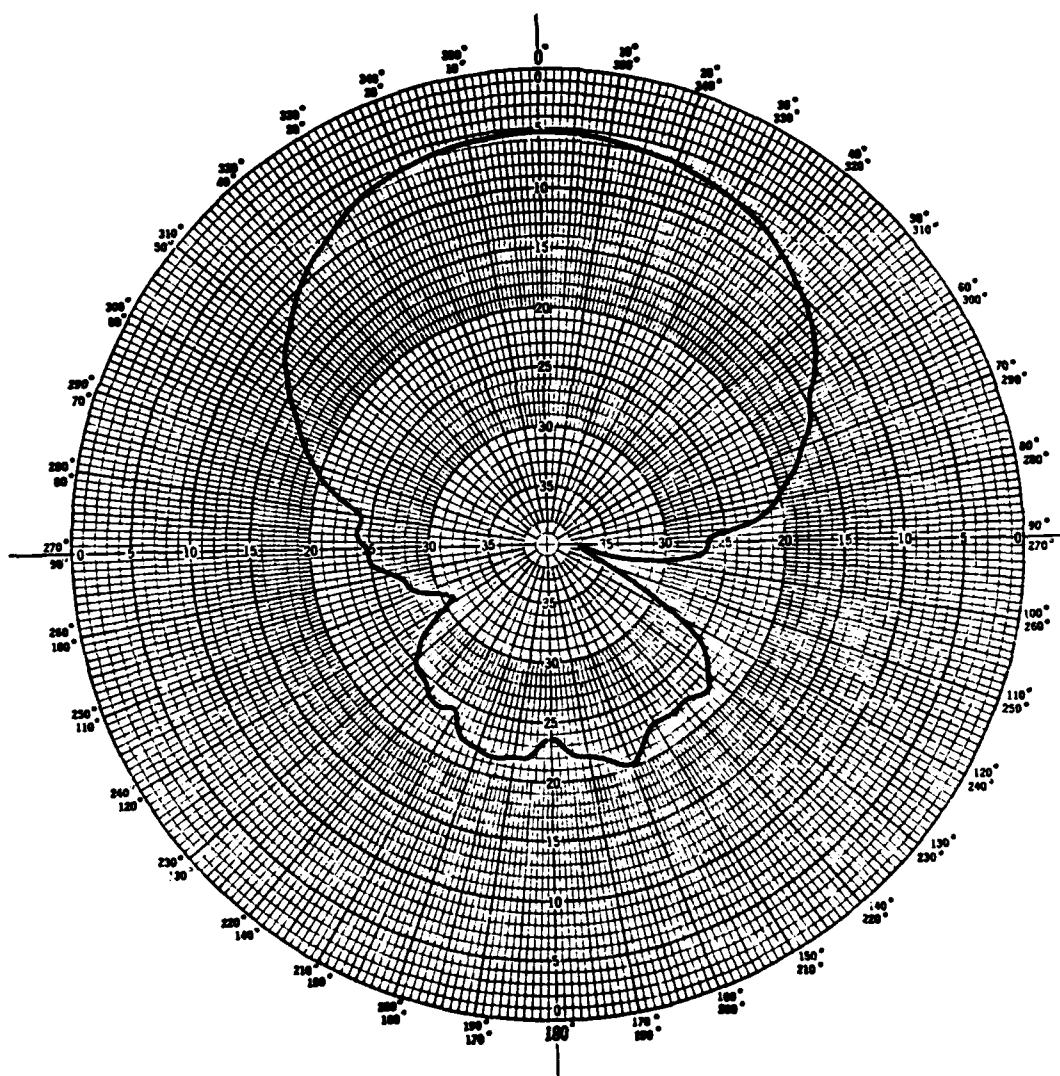
24 Jan 86
7.0 GHz Patch
H-Plane Pattern



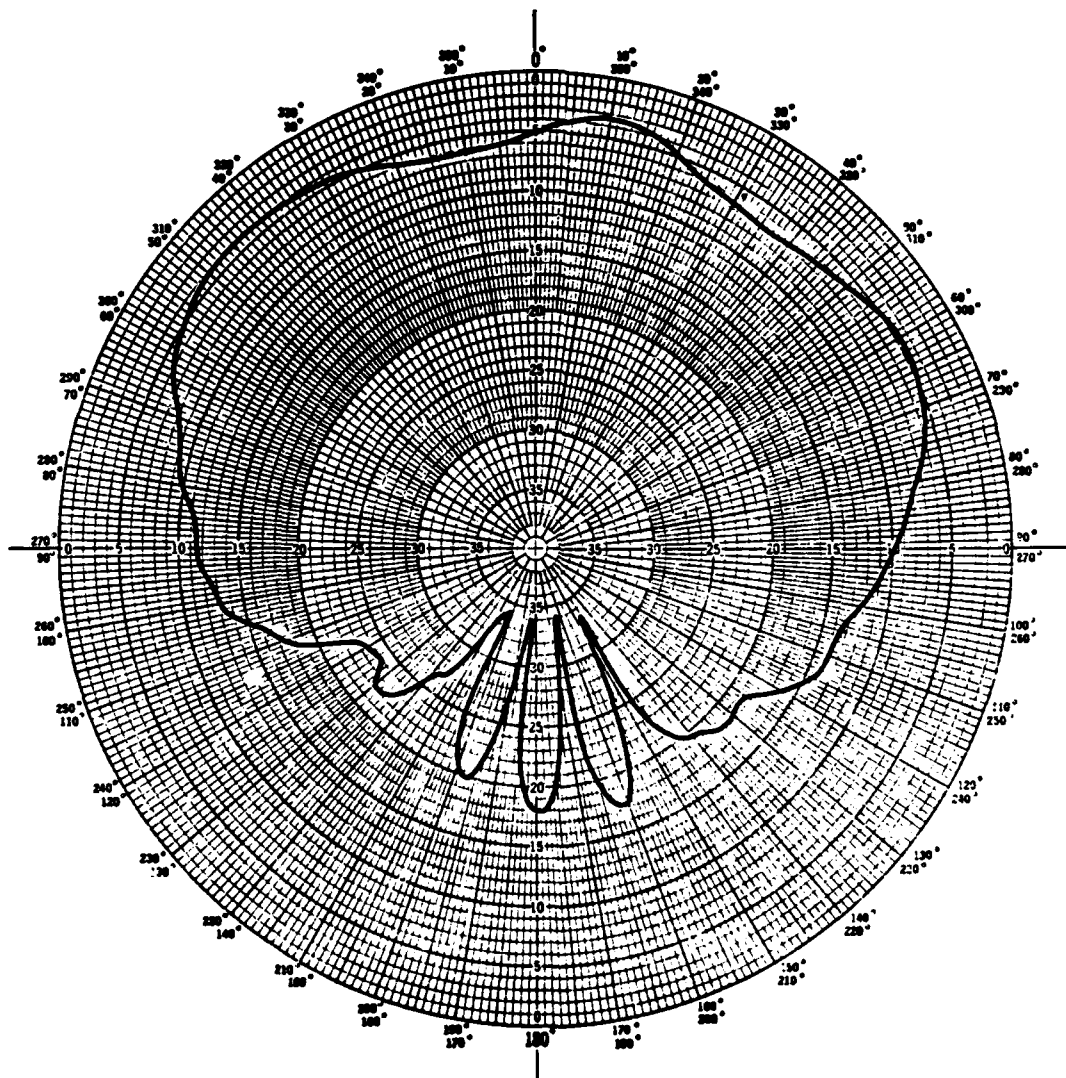
27 Jan 86
7.0 GHz Patch
E-Plane Pattern



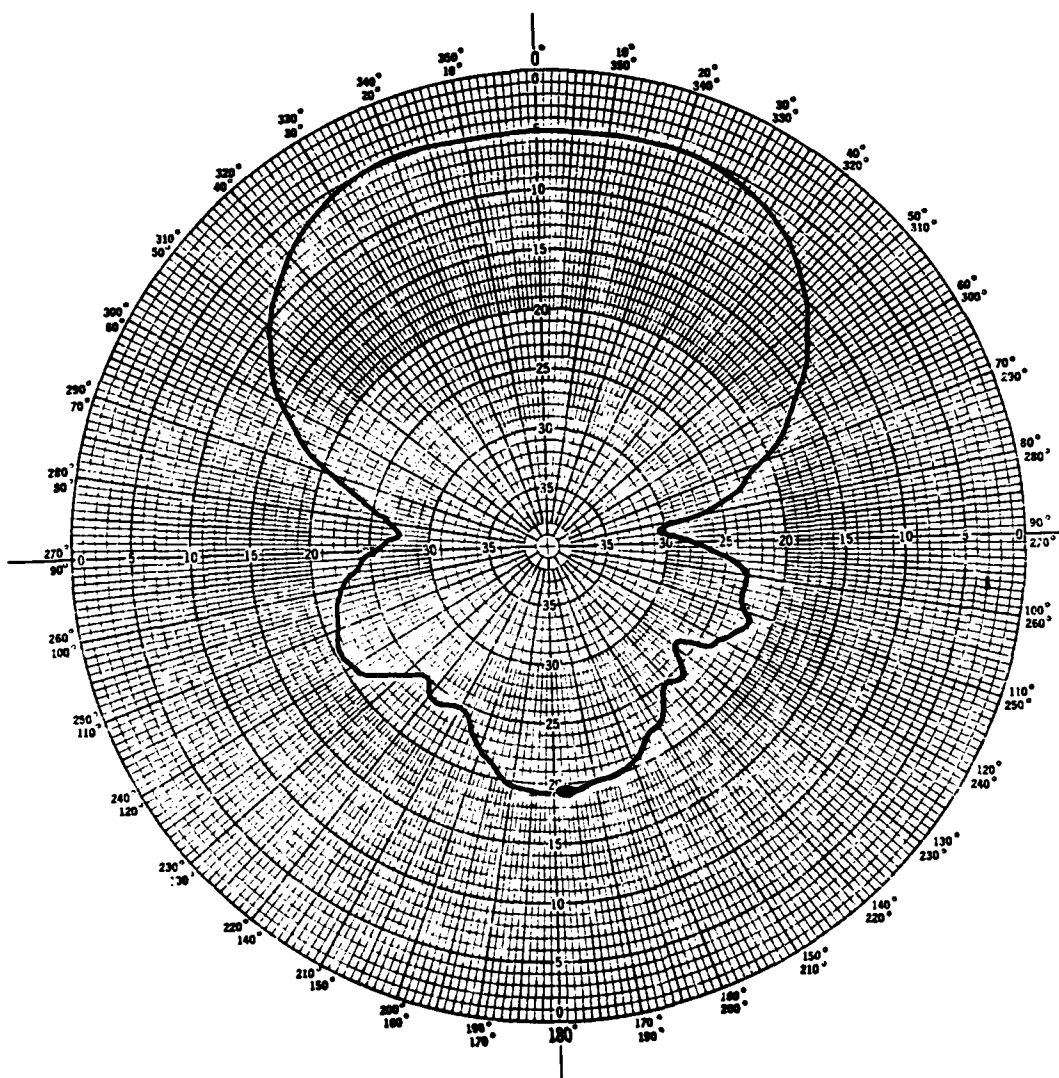
24 Jan 86
8.0 GHz Patch
H-Plane Pattern



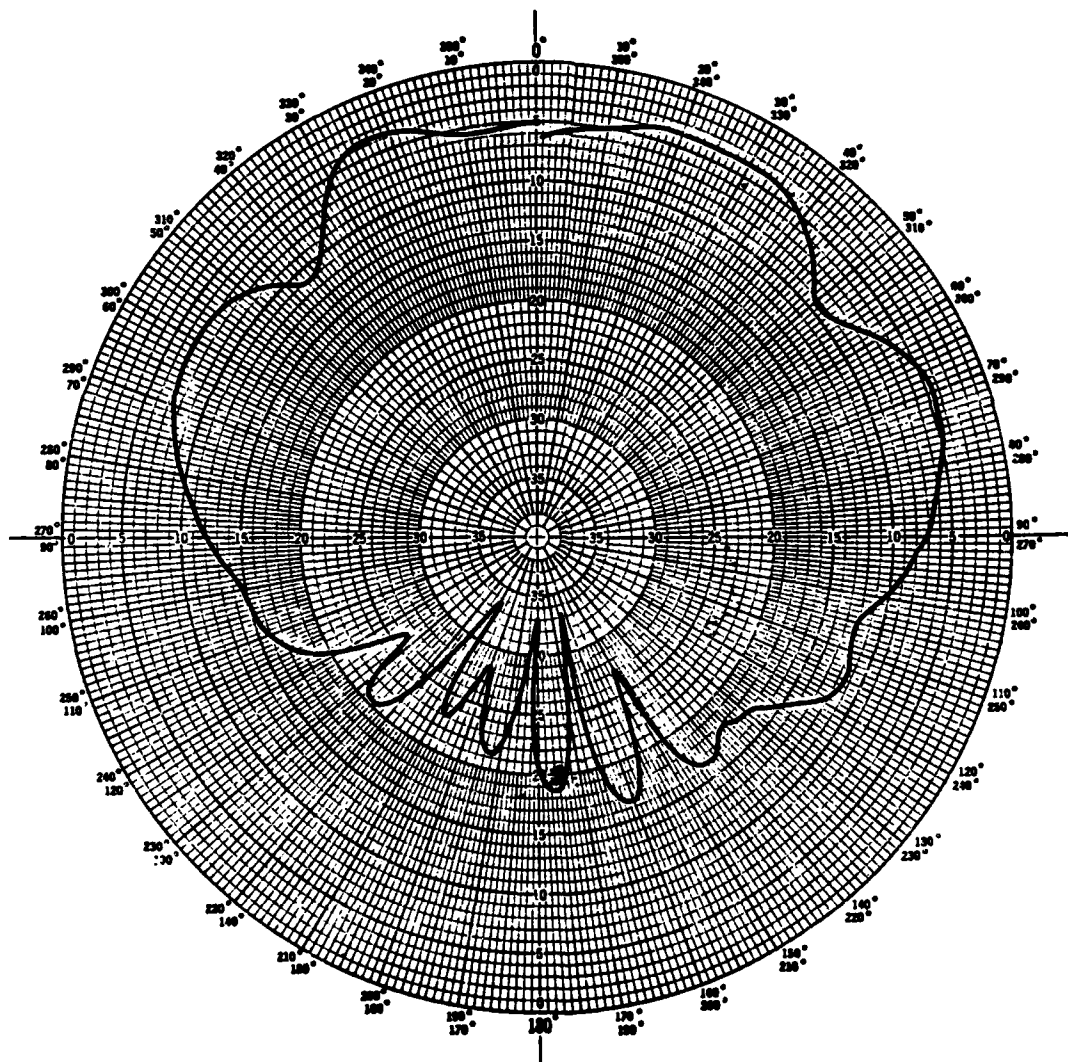
27 Jan 86
8.0 GHz Patch
E-Plane Pattern



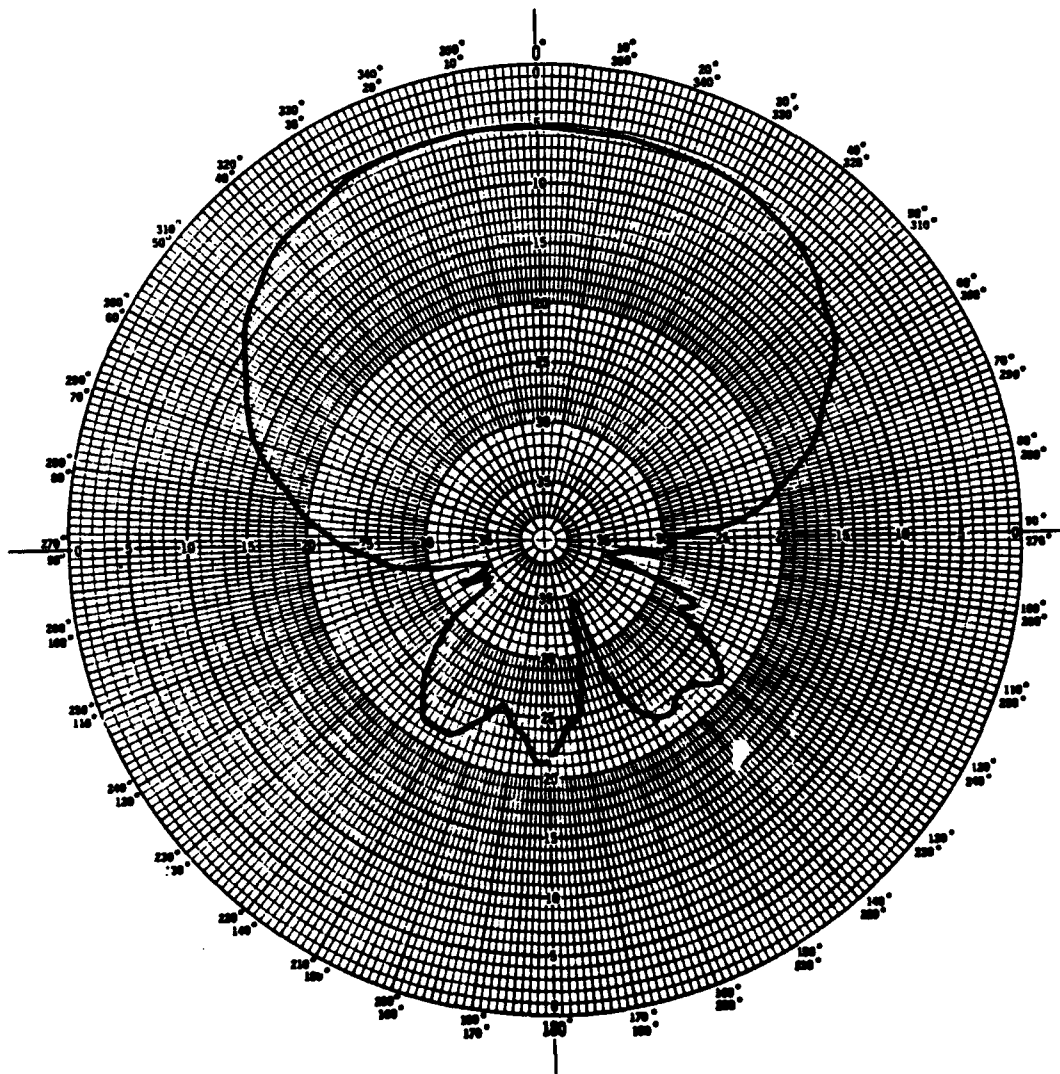
27 Jan 86
9.0 GHz Patch
H-Plane Pattern



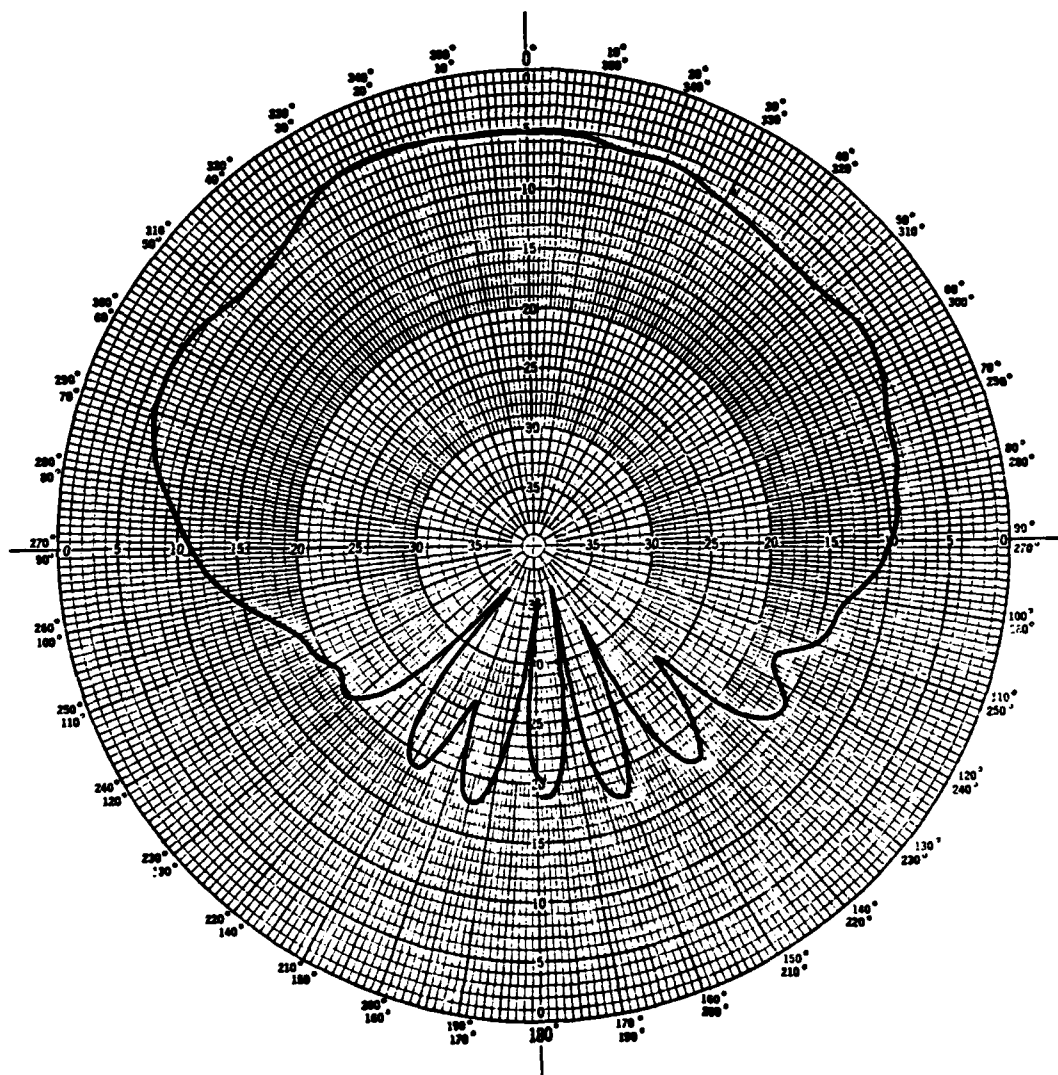
27 Jan 86
9.0 GHz Patch
E-Plane Pattern



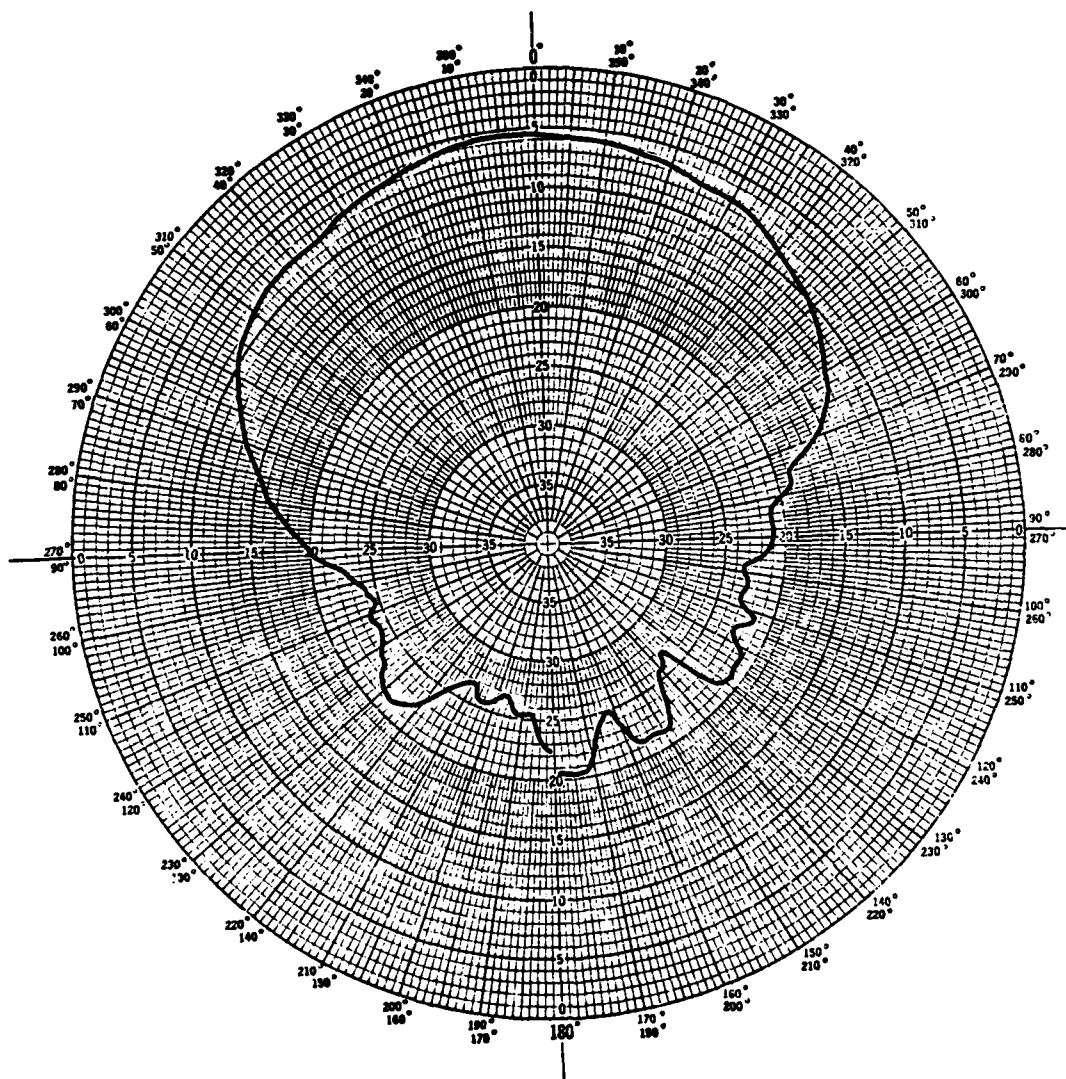
27 Jan 86
10.0 GHz Patch
H-Plane Pattern



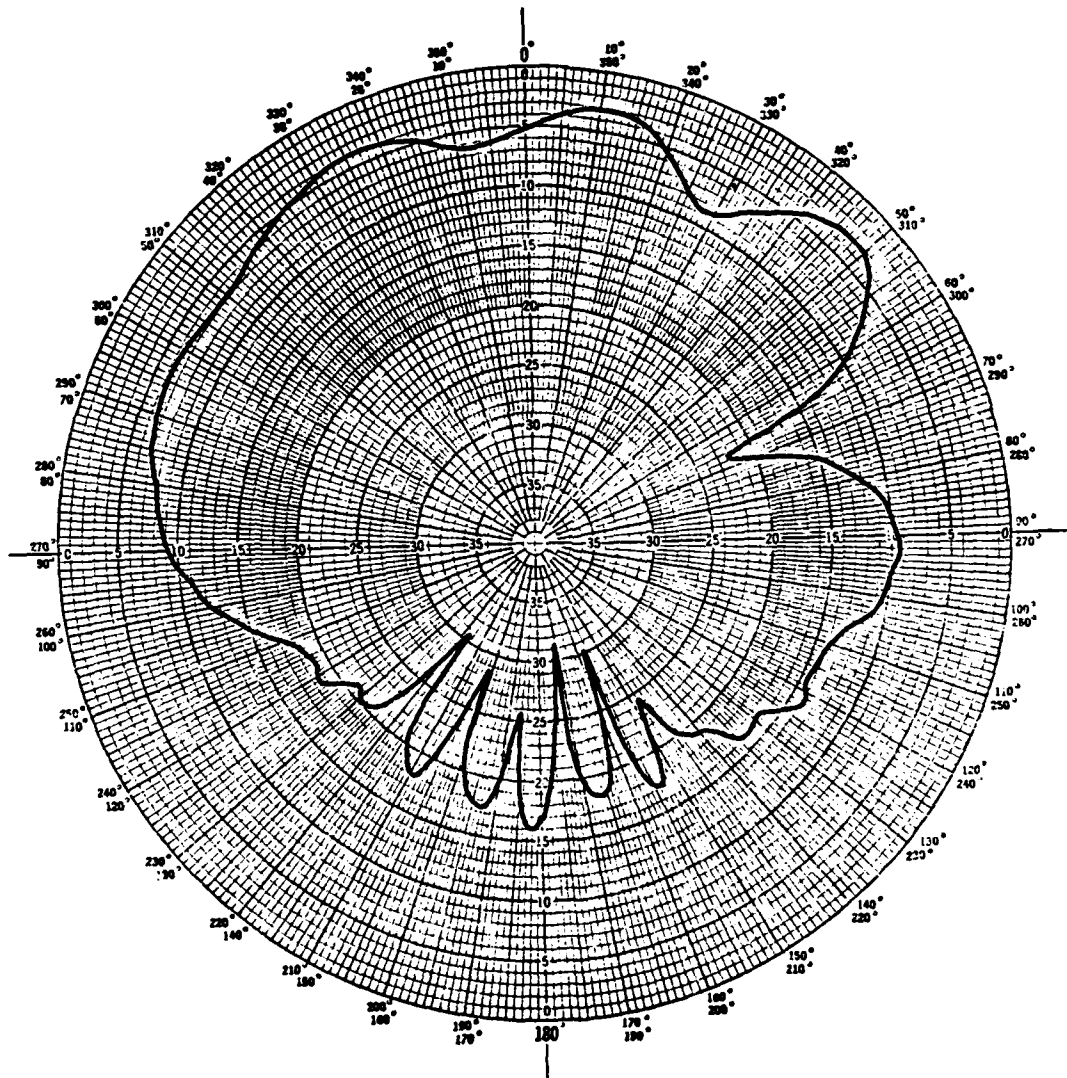
27 Jan 86
10.0 GHz Patch
E-Plane Pattern



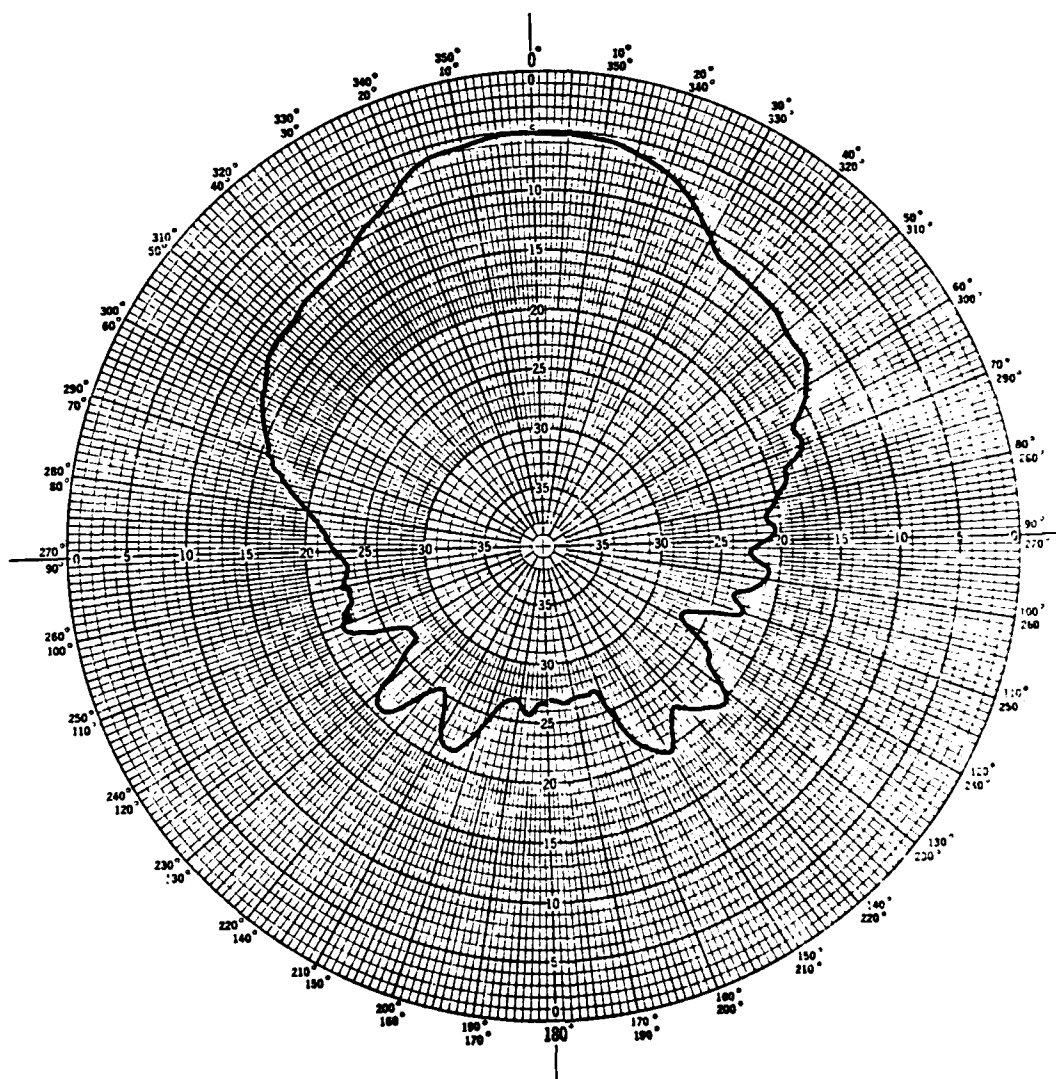
27 Jan 86
11.0 GHz Patch
H-Plane Pattern



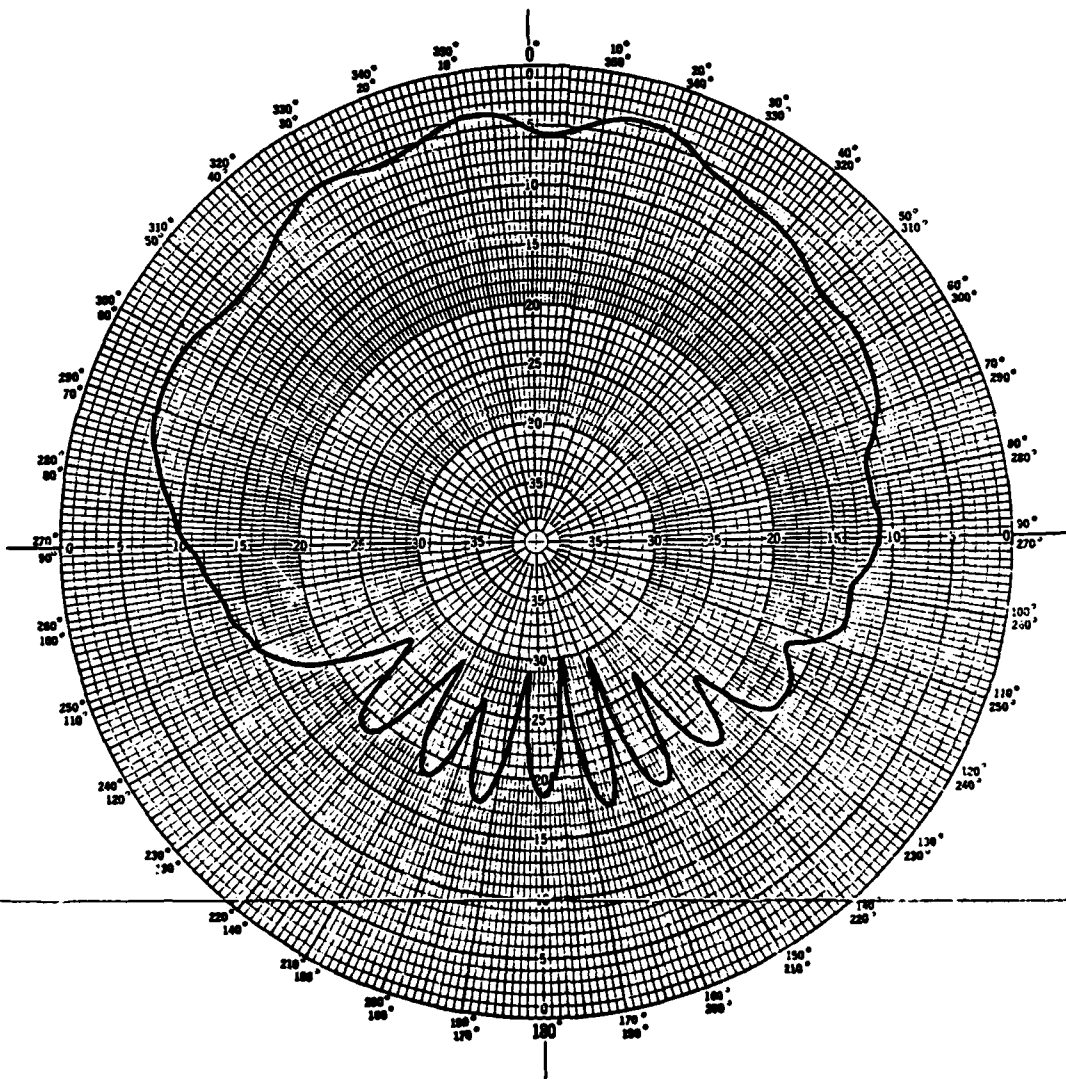
27 Jan 86
11.0 GHz Patch
E-Plane Pattern



27 Jan 86
12.0 GHz Patch
H-Plane Pattern



27 Jan 86
12.0 GHz Patch
E-Plane Pattern



*MISSION
of
Rome Air Development Center*

RADC plans and executes research, development, test and selected acquisition programs in support of Command, Control, Communications and Intelligence (C³I) activities. Technical and engineering support within areas of competence is provided to ESD Program Offices (POs) and other ESD elements to perform effective acquisition of C³I systems. The areas of technical competence include communications, command and control, battle management, information processing, surveillance sensors, intelligence data collection and handling, solid state sciences, electromagnetics, and propagation, and electronic, maintainability, and compatibility.

END

5-87

DTIC